

# Population Syntheses for Neutron Star Systems with Intrinsic Kicks

Chris Fryer, Adam Burrows, and Willy Benz  
Steward Observatory, University of Arizona, Tucson, AZ 85721

## ABSTRACT

We use a Monte Carlo binary synthesis code to model the formation and evolution of neutron star systems including high-mass X-ray binaries, low-mass X-ray binaries, double neutron star systems and radio pulsars. Our focus is on the signature imprinted on such systems due to natal kicks to neutron stars over and above that imparted by orbital motions. The code incorporates the effect of the galactic potential (including rotation) on the velocities of these systems. A comparison between our models and the observations leads us to infer mean natal kicks  $\gtrsim 400 - 500$  km/s. Moreover, to be consistent with all the data, we require a bimodal kick distribution with one peak in the distribution near 0 km/s and the other above 600 km/s.

*Subject headings:* stars: neutron; pulsars; supernova; binaries

## 1. Introduction

Support for the claim that many neutron stars move with high velocities continues to mount. Probably the most compelling evidence lies in the transverse velocities of the radio pulsar population. With the most recent proper motion measurements and the newly-corrected distance determinations of Taylor & Cordes (1993), Lyne & Lorimer (1994) have derived a mean pulsar velocity of 450 km/s, an increase of almost a factor of 2 over previous estimates. Velocities above 800 km/s have been inferred by associating pulsars with supernova remnants (Caraveo 1993; Frail, Goss & Whiteoak 1994 although see Gaensler & Johnston 1995) and from observations of the bow shocks produced by neutron stars as they plow through the interstellar medium (Cordes, Romani, & Lundgren 1993). Neutron star kicks have been invoked to explain characteristics of O/B runaway stars (Leonard & Dewey 1992), double neutron star (DNS) systems such as PSR B1913+16 and PSR B1534+12 (Flannery & van den Heuvel 1975; Burrows & Woosley 1986; Yamaoka, Shigeyama, & Nomoto 1993; Fryer & Kalogera 1997), the non-zero angle between the spin and orbit axes of some recycled pulsar systems (Kaspi *et al.* 1996; Wasserman, Cordes, & Chernoff 1996), galactic gamma-ray bursters (Colgate & Leonard 1994; Podsiadlowski, Rees, & Ruderman 1995; Lamb 1995), and highly eccentric Be/NS binaries (van den Heuvel & Rappaport 1986).

Distilling the actual kick imparted to neutron stars from the pulsar velocities requires the delicate removal of the forces that have modified the pulsar motion since birth. For example, if the progenitor of the pulsar was in a binary system prior to the supernova explosion which formed the pulsar, then the binary rotational velocity would affect the final pulsar motion. In addition, escape from the binary potential, the effects of galactic rotation and the motion through the galactic potential all modify the pulsar velocities. The most reliable approach to this distillation process is the simulation of the pulsar velocity distribution given a kick distribution and a model for the binary and galactic effects. Using Monte Carlo binary population synthesis simulations, Dewey & Cordes (1987) found that 100 – 150 km/s kick velocities were required to explain the pulsar transverse-velocity distribution with the old distance measurements. More recently, Iben & Tutukov (1996) have claimed that this old pulsar transverse-velocity distribution can be

explained by binary effects alone. Iben & Tutukov use much more detailed binary population synthesis code which includes the synthesis of low-mass X-ray binaries (LMXBs) and high-mass X-ray binaries (HMXBs) (Iben, Tutukov, & Yungelson 1996a, 1996b) but which does not include the effects of neutron star kicks. To explain the transverse velocity distribution of pulsars using the *latest* proper motion measurements and the *newest* distance corrections, our calculations which include binary and galactic effects require large neutron-star kicks ( $> 400$  km/s).

The radio pulsar velocity data alone provide evidence for kicks, but they are unable to restrict the kick distribution itself. We show that Maxwellian distributions, flat distributions, even a delta function kick distribution, will match the observed radio pulsar data. To learn more about the kick distribution, we follow the approach of Iben & Tutukov (1996) and expand our study to include additional neutron star populations: low-mass X-ray binaries (LMXBs), high-mass X-ray binaries (HMXBs), DNSs, and globular cluster neutron stars. Naturally, any kick distribution is also restricted in that it must produce roughly the correct numbers of each of these neutron star systems. High kicks will overcome the gravitational potential of binaries and globular clusters preventing the formation of LMXBs, HMXBs, DNSs and globular cluster neutron stars. Our basic approach is to calculate the minimum birthrate of each type of these systems based on the observations and the maximum birthrate derived from our Monte Carlo code for a given kick distribution which fits the pulsar velocity distribution. If this maximum birthrate is less than the observed minimum, we can “conservatively” conclude that the input kick distribution, although it fits the pulsar velocity distribution, is not the correct kick distribution. Employing the constraints of all these systems, we can rule out many of the kick distributions in the literature (Kalogera & Webbink 1996a - hereafter KW96; Brandt & Podsiadlowski 1995). We do find that a two-population pulsar velocity distribution is able to fit the current observations and our best-fitting double-peaked distribution has one peak near  $\sim 625$  km/s and the other near 0 km/s<sup>1</sup>. This bimodal kick distribution is a challenge to any theory of kick origins.

In §2, we discuss the observed pulsar distribution and our method to limit the effects of biases. We then outline our technique to compare our simulations to the data. We repeat this process for the neutron stars in globular clusters and the massive binary systems. In §3, we describe the various uncertainties in our population synthesis calculations and show the dependence of our results on the many poorly constrained binary population synthesis parameters. In §4, we discuss the results and implications of these new simulations and the constraints they place on the neutron star kick velocity distribution. We conclude with a discussion of our results.

## 2. Neutron Star Populations

We determine possible nascent neutron star kick distributions by combining the radio pulsar proper motion data with the retention fraction of neutron stars in globular clusters and the formation rates of LMXBs, HMXBs, DNSs. We begin by discussing the birthrate comparisons for the massive binary systems and conclude this section discussing the globular retention fraction, pulsar velocity distribution, and lastly, the formation mechanisms of O/B runaway stars.

For the binary populations, we must carefully determine the birthrate (BR) of each type of binary

---

<sup>1</sup> The peak near 0 km/s may be significantly broadened and still satisfy our constraints. A flattened distribution ranging from 0 km/s - 200 km/s will fit the data equally well.

system, given by:

$$BR = \frac{\text{Number of Systems}}{SN} \times \frac{SN}{yr} \times f_{binary}. \quad (1)$$

Using our Monte Carlo code, we simulate  $10^6$  binary systems and calculate the number of each type of system produced and the total number of supernovae ( $SN$ ), from which we derive the first term in equation (1). By assuming a supernova rate ( $SN/yr$ ) and the fraction of systems in binaries,  $f_{binary}$ , we calculate the birthrate of each type of system.

The birthrate itself can not be easily compared with the observations. Hence, we resort to a variety of indirect techniques to constrain the models. Since we use a different technique for each type of system, we discuss each of them separately. When we encounter any uncertainty in a calculation, we choose the conservative bound such that our simulated birthrates are always upper limits.

There are a number of ways to estimate formation rates of massive systems, the most direct being the supernova rate. To compare our rates with the recent population synthesis work, we list the supernova rates of previous population synthesis work given the assumptions in their calculations: KW96 -  $\sim 7.7 \times 10^{-3} \text{ SN yr}^{-1}$ , Dalton & Sarazin (1995 - DS95) -  $\sim 7 \times 10^{-3} \text{ SN yr}^{-1}$ , and Iben, Tutukov & Yungelson (1996a, 1996b) -  $\sim 9.1 \times 10^{-3} \text{ SN yr}^{-1}$ . However, galactic SN rates themselves are typically estimated to be in the range  $10^{-2} - 3 \times 10^{-2} \text{ SN yr}^{-1}$  (Tammann, Loeffler, & Schroeder 1994). To be consistent the results of Tammann *et al.* (1994), while choosing a value close to the recent binary population synthesis work, we assume a supernova rate of  $10^{-2} \text{ SN yr}^{-1}$  for our simulations. The binary fraction ( $f_{binary}$ ) depends upon the mass ratio distribution of binaries that we adopt. We discuss the various mass ratio distributions and their resultant binary fractions in §3.

### 2.1. Low-Mass X-ray Binaries

The X-ray emission of an LMXB is powered by Roche-lobe overflow from its low-mass companion (Iben, Tutukov, & Yungelson 1996b). Although a necessary condition for LMXB creation is that the low-mass companion remain bound to the neutron star after the supernova explosion, this condition is not sufficient. The bound system must evolve to a phase in which stable Roche-lobe overflow occurs. For our simulations, we use the technique outlined by KW96. We evolve the orbital separation by both gravitational radiation and magnetic braking. Using the results of Kalogera & Webbink (1996b), we restrict our sample to those systems that develop stable sub-Eddington or super-Eddington accretion. Since systems with super-Eddington accretion may not be observed as LMXBs and since systems with super-Eddington accretion rates are an order-of-magnitude more numerous than sub-Eddington accretion, the inclusion of super-Eddington systems may overestimate the birthrate of LMXBs by over a factor of 10.

The astute reader may worry that our simulations do not consider all of the possible formation scenarios for LMXBs and, hence, that we are underestimating their formation rate. Our simulations include the standard formation scenario which uses a common-envelope phase to tighten the pre-SN orbit (van den Heuvel 1983). In addition, we include scenarios which use the kick to reduce the orbital separation after the supernova without the aid of a common-envelope phase (Kalogera 1996). We do not include any scenarios involving a Thorne-Żytkow phase (Eggleton & Verbunt 1986). Models of common-envelope evolution (Chevalier 1993, Brown 1995, Fryer, Benz, & Herant 1996) show that the neutron star would collapse into a black hole before it could spiral into the core of its companion to form a Thorne-Żytkow object. Similarly, we ignore the accretion-induced collapse (AIC) route to LMXBs. Simulations by Woosley

& Baron (1992) limit the total rate of AICs to  $10^{-4} \text{ yr}^{-1}$  to avoid nucleosynthetic contamination by their ejecta. This rate is comparable to the rate predicted by Iben, Tutukov, & Yungelson (1996b), who conclude that AICs make up no more than a few percent of the LMXB population. In addition, recent simulations by Fryer *et al.* (1997) suggest an upper limit on the total AIC rate an order of magnitude lower than that of Woosley & Baron. Hence, it is unlikely that AICs contribute to the LMXB population.

Using our Monte Carlo calculations, we determine the number of LMXBs formed per supernova (the first term in equation 1). To compare with the observations, we would like to multiply our birthrate with the lifetime of our LMXBs to derive the number of galactic LMXBs. However, the lifetime of an LMXB is very difficult to estimate. We instead calculate an upper limit to the X-ray flux of these systems collectively by assuming that the low-mass companion is completely consumed by the neutron star and that all of the energy from mass accretion is converted into X-ray photons. This galactic luminosity is:

$$L_X^{tot} = \frac{GM_{NS}}{R_{NS}} \times \sum_{M_{co}} BR(M_{co}) \times M_{co}, \quad (2)$$

where  $G$  is the gravitational constant,  $M_{co}$  is the mass of the companion which is accreting onto the neutron star, and  $M_{NS}$  and  $R_{NS}$  are the mass and the radius of the neutron star, respectively.  $BR$  is the LMXB birthrate calculated in our Monte Carlo simulations (eq. 1). KW96 estimate the X-ray flux from galactic LMXBs to be  $L_{X,tot} \sim 1.7 \times 10^{39} \text{ erg s}^{-1}$ . In §4, we make use of the fact that we have overestimated both the LMXB formation rate and the LMXB X-ray emission. If, for a given kick distribution, our calculated upper limit falls below the observed value, that kick distribution is excluded.

## 2.2. High-Mass X-ray Binaries

HMXBs are thought to be powered by material from the massive companion’s wind. For these systems, we use the same technique as DS95. Using the models of Schaller *et al.* (1992), we determine the high-mass companion’s radius, its mass loss rate, and wind velocity as a function of the companion’s age, from which we can estimate the mass accretion rate onto the neutron star as a function of time (see DS95). Then the maximum X-ray luminosity of each HMXB can be estimated:

$$L_X = \frac{G\dot{M}_{acc}M_{NS}}{R_{NS}} \quad (3)$$

where  $\dot{M}_{acc}$  is determined in the same manner as in DS95. DS95 introduce an efficiency parameter for the conversion of potential energy into X-ray photons, but we assume, as we do in the case of LMXBs, that the conversion is 100% when calculating an upper limit to the formation rate of HMXBs.

Using the Schaller *et al.* (1992) models, we not only calculate the X-ray luminosity, but the HMXB lifetime. For HMXBs, we can combine our estimated birthrate with this lifetime to determine a total HMXB population. We compare our brightest sources with the bright galactic sources. Meurs & van den Heuvel (1989) estimate the number of HMXBs with  $L_X > 10^{36} \text{ erg s}^{-1}$  to be  $55 \pm 27$ . We will require the upper limit from our simulations to give  $N(L_X > 10^{36} \text{ erg s}^{-1}) \gtrsim 28$ . As in the case for LMXBs, if our simulated upper limit falls below the lower limit in the observations, we conclude that the kick distribution does not fit the data.

### 2.3. Double Neutron Star Systems

We calculate the birthrate of DNSs by including all bound double neutron star systems. This simple prescription is suggested by the fact that there are many opportunities during the evolution of these systems to tighten their orbits and recycle their pulsars. van den Heuvel & Lorimer (1996) estimate that the formation rate for DNS systems whose merger timescale is less than a Hubble time is  $\sim 8 \times 10^{-6} \text{y}^{-1}$ , but previous estimates were as low as  $1 - 3 \times 10^{-6} \text{y}^{-1}$  (van den Heuvel 1995, Curran & Lorimer 1995). Since we are interested in estimating an upper limit on the theoretical birth rate, we require only that our total number of bound DNS systems be greater than the  $\sim 10^{-6} \text{y}^{-1}$  predicted by the observed close binary systems.

Alternate scenarios for double neutron star formation do exist. In globular clusters, a viable formation scenario for DNSs such as PSR 2127+11C involves stellar collisions with binaries in cluster cores (Anderson *et al.* 1990). This scenario is not a likely formation mechanism for the galactic disk DNSs. Brown (1995) has suggested an alternate formation scenario which includes a double helium star phase. This mechanism requires that the binary components have nearly equal masses. Our code models these systems, but for the mass-ratio distributions we use (see §3), this mechanism provides a negligible contribution to our DNS formation rate.

### 2.4. Globular Clusters

Rather than calculate a birthrate of neutron stars in globular clusters, we simply estimate their retention fraction for a given kick velocity. The large population of neutron stars observed in globular clusters requires that a sizable fraction ( $> 1 - 10\%$ ) of their neutron stars remain bound to the cluster (Bhattacharya & van den Heuvel 1991). If they form primarily from core-collapse supernova in situ, then the retention fraction places useful constraints upon the neutron-star kick distribution. An alternate formation mechanism in globular clusters involves the accretion-induced collapse of white dwarfs (e.g. Bailyn & Grindlay 1990). The role AICs play in globular clusters is restricted, just as with LMXBs, by the nucleosynthetic yields predicted by Woosley & Baron (1992) and Fryer *et al.* (1997). Bailyn & Grindlay (1990) require an AIC rate close to  $10^{-4} \text{y}^{-1}$  to explain the neutron stars in globular clusters, an order of magnitude higher than the upper limit given by Fryer *et al.* (1997). It is therefore unlikely that AICs make up more than about 10% of the neutron stars in globular clusters.

However, if neutron stars created through core-collapse explosions do indeed receive large kicks, Drukier (1995) has shown that the retention fraction of these neutron stars can be quite low ( $\lesssim 1\%$  of the neutron stars formed). We use the retention fractions versus neutron-star velocity derived by Drukier (1995) to determine the retention fractions of neutron stars (both bound and unbound systems) for all of our kick distributions. Drukier uses both Fokker-Planck and Mitchie-King models to simulate the range of globular cluster retention fractions and includes specific models for NGC 6397 and  $\omega$  Cen. Our limit for a satisfactory neutron-star kick distribution requires that 1% of the neutron stars formed (both binary systems and single stars are considered) in NGC 6397 remain bound. We calculate the entire range of retention fractions derived using the Drukier models.

## 2.5. Radio Pulsars

The primary constraint on the neutron star kick distribution are the pulsar transverse velocities. The high velocities, as we show in §4, require high-velocity kicks. Given the strong dependence of our results upon the proper motion velocities, we must first discuss the many uncertainties surrounding any interpretation of this data. We conclude this section with a discussion of our simulations.

### 2.5.1. Observations and Uncertainties

The current database of pulsars with proper motions now contains well over 100 pulsars (Taylor, Manchester, & Lyne 1993). However, this sample contains many biases and uncertainties (Iben & Tutukov 1996; Hansen & Phinney 1997; Cordes & Chernoff 1997). In this section, we discuss many of the uncertainties and biases listed in the literature and describe our method to limit their effects.

Our pulsar sample is taken from the proper motion data of Taylor, Manchester, & Lyne (1993) with distances determined using the new electron density model of Taylor & Cordes (1993). For some pulsars, the distances estimated from the new electron density model are over a factor of two greater than their old predictions. Alternate distance estimation techniques provide some support for the Taylor & Cordes distances, but there exist specific cases, such as PSR J0738-4042, where the preferred distance is 5 times smaller than that predicted by the electron density model (Johnston *et al.* 1996). The distance estimated by Taylor & Cordes for PSR J0738-4042 was quite high ( $> 11$  kpc). By restricting our sample to the radio pulsars within 5 kpc of the sun, we hope to avoid the most grievous distance errors. Nonetheless, distance measurement errors are a major concern and we will discuss their effect on our results in §4.

Aside from uncertainties in the distance estimates, we must be careful to avoid any biases in our radio pulsar sample. A clear selection bias is that very high-velocity pulsars rapidly leave the galactic disk and can even escape the galactic potential. Low-velocity pulsars, on the other hand, remain bound to the disk and are easily detected. We avoid this bias by limiting our sample to the young radio pulsar population ( $t_{age} = P/2\dot{P} < 3 \times 10^6$  y). In addition, by restricting our sample to those pulsars whose ages are less than the typical luminosity decay times (Gunn & Ostriker 1970), we avoid uncertainties in the pulsar age-luminosity relation.

Iben & Tutukov (1996) have suggested that there may be a bias against low velocity pulsars. The proper motion of a distant, low-velocity pulsar is difficult to determine. Iben & Tutukov (1996) have claimed that there is a trend in the data supporting this hypothesis (see Figure 1). This bias is not real, but instead is probably due to errors in the distance estimates and is akin to the luminosity/velocity relation suggested by Tutukov, Chugai, & Yungelson (1984) and Hansen & Phinney (1997). They noted a clear trend in the data showing that the lowest velocity pulsars have lower luminosities. By realizing that  $v_{trans} \propto \text{proper motion} \times \text{distance}$  and that  $\text{Luminosity} \propto \text{distance}^2$ , Dewey & Cordes (1987) argued that this trend was not a bias, but a consequence of distance errors. This effect is illustrated in Figure 2. Distance errors also explain the trend upon which Iben & Tutukov (1996) base their selection bias (see Fig. 3). By misinterpreting these trends as true biases rather than straightforward distance errors, Tutukov, Chugai, & Yungelson (1984), Iben & Tutukov (1996), and Hansen & Phinney (1997) predict much lower mean pulsar velocities ( $\sim 100 - 300$  km/s) than those predicted by Lyne & Lorimer (1994). Given that the Dewey & Cordes (1987) argument fits the observations so well (Figs. 2,3), the bias is not likely to be true,

and hence, like Lyne & Lorimer (1994), we do not correct for it.<sup>2</sup>

Thus, we limit our data both in distance ( $< 5\text{kpc}$ ) and age ( $t_{age} < 3 \times 10^6 \text{ y}$ ), taking only those pulsars which satisfy both of these constraints. Unfortunately, this limits our sample of pulsars to 27 pulsars with proper motion estimates. Figure 4 shows the distribution of transverse velocities for this sample where we have smoothed the data by assuming a distance error of 30%.

### 2.5.2. Models

Our results rely upon several assumptions about the kick distribution: that it is isotropic and it does not depend upon the binary nature of the exploding star (i.e. The kick distribution for neutron stars formed in binary systems is identical to the distribution for neutron stars formed in supernova explosions of single stars.). Using Monte Carlo statistics, we compare our simulated pulsar population<sup>3</sup> to the radio pulsar sample, constrained by our age ( $t_{age} < 3 \times 10^6 \text{ y}$ ) and distance ( $D_{sun} < 5 \text{ kpc}$ ) limits. For each kick distribution, we calculate a pulsar velocity distribution with our population synthesis code which includes both binary systems and single stars. To calculate the transverse velocity distribution to compare with the observations, we must follow the motions of the pulsars in a galactic potential.

We use the galactic potential of Miyamoto and Nagai (1975)

$$\Phi(R, z) = \frac{GM_{gal}}{(R^2 + [a + (z^2 + b^2)^{1/2}]^2)^{1/2}} \quad (4)$$

where  $R$  is the distance from the galactic center in the plane of the disk,  $M_{gal}$  is the mass of the galaxy,  $z$  is the distance off the disk and  $G$  is the gravitational constant. We use fits by Miyamoto and Nagai for  $a$  and  $b$  ( $a = 7.258\text{kpc}$  and  $b = 0.520\text{kpc}$ ). We normalize  $M_{gal}$  by insuring that the rotational velocity of the sun at 8.5 kpc is 225 km/s.

We distribute our initial binary systems randomly following the O/B disk population (Mihalas & Binney 1968) with a disk scale length of 3.5 kpc and a scale height and cutoff out of galactic plane of 60 pc and 300 pc, respectively. The motion of each system consists of a component from the galactic rotation and a randomly oriented velocity due to binary and kick effects. Figure 5 shows the effects, first of binary evolution, and then the effects of the galactic potential including rotation, upon a kick distribution. The effect of the galactic potential not only leads to significant changes in the mean pulsar velocity (for some kick distributions, the deviation can be as high as 50%), but it drastically alters the pulsar velocity distribution and can not be ignored.

We use the Kolmogorov-Smirnov test to derive the probability that the simulated pulsar velocity distribution, subject to the same age and distance constraints as our observed sample, is not from the same parent population as the radio-pulsar sample. We repeat the test using the extreme possible velocities for each pulsar (by including both distance and proper motion errors<sup>4</sup>). As a secure limit, we exclude only

---

<sup>2</sup>However, the current sample of pulsar proper motions is far from complete and many of the issues that Hansen & Phinney (1997) bring up may prove to be important.

<sup>3</sup> unbound neutron stars produced in our synthesis calculations either because their progenitor was a single star or because they became unbound during the supernova explosion in the binary system

<sup>4</sup>Note that nearly 20% of the pulsars have proper motion errors greater than the measured value. That is, their proper motions are, within the errors, zero. (Taylor, Manchester, & Lyne 1993)

those distributions where this probability is greater than 99%.

## 2.6. O/B runaway stars

O/B runaway stars are O or B stars that have been given high space velocities. One proposed mechanism for O/B runaway stars is ejection during a supernova event (Blaauw 1961). However, this mechanism requires that the O/B runaway stars remain bound to the newly-formed neutron star (Leonard 1990, Leonard & Dewey 1992) and the current observational evidence suggests that most O/B stars are not in close binaries (Gies & Bolton 1986, Sayer, Nice & Kaspi 1996, Philp *et al.* 1996). An alternate formation mechanism for these objects is dynamical ejection in cluster environments (Leonard 1995) and this mechanism may well explain most O/B runaway stars. Because no standard model exists for the formation of these objects, we do not use them as a constraint for our kick distributions. In the conclusions, we briefly address these objects in the context of our derived kick distribution.

## 3. Simulations

To determine the birthrate of each type of neutron star system, we first calculate the number of systems formed per supernova, the first term in equation (1). To calculate this term, we have created a Monte Carlo population synthesis code which chooses from a range of initial conditions and then evolves the binary system through one, and if the secondary mass is sufficiently high, a second supernova explosion. A variety of uncertainties and “free-parameters” (both in the initial conditions and in the subsequent binary evolution) results in a broad range of birthrates. Therefore, to attack the problem of neutron star kicks, we must explore the realistic range in these rates. In this section, we present the results of an intensive study of the effects of the initial conditions and free parameters on the production rates of LMXBs, HMXBs and DNSs, and on the radio pulsar velocity distribution. The results for the different populations are summarized in Figure 6. Although the birthrates for these systems can change by over an order of magnitude as we vary the parameters, if the kick is sufficiently strong, it will dominate the pulsar velocity distribution (Figure 7). The mean pulsar velocity, using a delta-function kick velocity of 200 km/s, after binary effects ranges from 199 km/s to 202 km/s. The velocity dispersion ranges from 11 – 15 km/s for all the binary parameters except if we vary the common envelope efficiency or mass loss. For a common envelope efficiency  $\alpha = 0.2$ , the dispersion is 5 km/s and for no mass loss, the dispersion is 22 km/s. The variation in the velocity dispersions is so small that, for the purposes of our simulations, any set of binary parameters will essentially give the same pulsar velocity distribution. (This is not the case when the kick magnitude becomes smaller than the average orbital velocity  $\lesssim 50$  km/s.)

### 3.1. Initial Conditions

Four parameters are required to describe a binary system. These are the masses of the two stars,  $M_{p,0}$  and  $M_{c,0}$ , the orbital separation,  $A_0$ , and the initial eccentricity,  $e_0$ . Unfortunately, for massive binaries, observational data only moderately constrain these parameters (Hogeveen 1991). Therefore, we are forced to consider a wide range of initial conditions and to use the neutron star binary production rates themselves to limit the initial conditions. The varying effects of these assumptions are summarized in Table 1, which lists the birthrates of LMXBs, HMXBs, and DNSs for 3 delta-function kick velocities and a standard set of



parameters. For each kick velocity, it also shows the effects of a variety of deviations from the standard parameter set.

### 3.1.1. Mass Ratios and the Initial Mass Function

In our simulations, we determine the initial mass of the primary ( $M_{p,0}$ ) by sampling an Initial Mass Function (IMF):

$$f(M_{p,0}) \propto M_{p,0}^{-\alpha_{IMF}}. \quad (5)$$

We retain  $\alpha_{IMF}$  as a free parameter, but must choose a minimum and a maximum neutron star forming primary mass. For most of our simulations, we use  $\alpha_{IMF} = 2.7$  (Scalo 1986) and primary mass limits of 10 and  $40M_{\odot}$ .

The companion mass distribution is much more difficult to determine. The standard technique prescribes a mass ratio ( $q = \frac{M_s}{M_p}$ ) distribution  $P(q)$  by

$$P(q) \propto q^{-\alpha_{MR}}. \quad (6)$$

Observational data for massive star binaries is limited and the effects of selection biases can be extreme. Garmany, Conti, and Massey (1980) claim a strong, bias-corrected, peak at  $q = 1$ . This led DS95 to choose  $\alpha_{MR} = -1$  for the bulk of their simulations. However, by accurately accounting for the selection biases, Hogeveen (1991) found that the Garmany *et al.* results vastly underestimate the number of low-mass companions. Hogeveen favors a mass ratio distribution which is peaked at low  $q$  values with  $\alpha_{MR} = 2.7$  which flattens to  $\alpha_{MR} = 0$  below some critical  $q = q_0$ . We use a range of values for  $\alpha_{MR}$  and  $q_0$ . In Table 1, we see that low values of  $\alpha_{MR}$  such as those given by Garmany, Conti, and Massey (1980) lead to a maximum in the DNS production rate. However, the higher value of  $\alpha_{MR}$  claimed by Hogeveen (1991) is required to explain the production rate of LMXBs. For most of our simulations we use the high  $\alpha_{MR} = 2.7$  value, and vary only the critical value  $q_0$ .

The binary fraction depends upon the choice for the mass ratio distribution parameters. For  $\alpha_{MR} = 2.7$  and  $q_0 = 0.35$ , Hogeveen (1991) gives a binary fraction of 35%. For  $\alpha_{MR} = 2.7$  and  $q_0 = 0.15$ , this value increases to  $\sim 65\%$ . For the mass ratio distributions derived by Garmany, Conti, & Massey (1980), we use their calculated binary fraction of 43%.

### 3.1.2. Orbital Parameters

The distribution of initial eccentricities and separations is also not well known for massive systems. For then initial orbital separation ( $A_0$ ), we assume with Kraicheva *et al.* (1979) that

$$P(A_0) \propto 1/A_0. \quad (7)$$

We use an inner separation of twice the initial primary radius and a range of outer separations ( $10^{4-6}R_{\odot}$ ). For initial eccentricity ( $e_0$ ), we choose two distributions:

$$P(e_0) = \delta(e_0) \quad (8)$$

and

$$P(e_0) = 1. \quad (9)$$

For most of our simulations, we use an outer separation of  $10^4 R_\odot$  and the eccentricity distribution of eq. (8). As can be seen in Table 1, the choice of these has very little effect upon the neutron star system production rates.

### 3.2. Stellar Models and Binary Evolution

We base our binary evolution calculations on stellar models of single stars, to which we add binary effects such as mass transfer and common envelope evolution. For stellar radii and masses at different evolutionary periods, we use the fits from KW96 of the massive stellar models of Schaller *et al.* (1992) and the helium star models of Habets (1985) and Woosley, Langer, & Weaver (1995). Although many aspects of binary evolution are not well understood, the uncertainties have, either rightly or wrongly, been lumped into a few categories. Chief among these are mass transfer, common envelope evolution, and stellar winds. The varying effects of these assumptions are summarized in Table 2, which lists the birthrates of LMXBs, HMXBs, and DNSs for 3 delta-function kick velocities and a standard set of parameters. For each kick velocity, it also shows the effects of a variety of deviations from the standard parameter set.

When the primary star overfills its Roche Lobe, mass transfer begins. For binary systems with mass ratio  $q < 0.4$ , we assume that there is no stable mass transfer (Webbink 1979; Yungelson & Tutukov 1991; van den Heuvel 1983) and that the system immediately goes into a common envelope. For systems with less extreme mass ratios, we assume, as did DS95, that the mass transfer is initially stable. When the two stars attain equal masses, it is assumed that the mass transfer is no longer stable and a common envelope phase begins.

For stable mass transfer, we follow the prescription of van den Heuvel (1995):

$$\Delta M_s = -\Delta M_p \times (1 - f_{trans}) \quad (10)$$

where  $\Delta M_s$ ,  $\Delta M_p$  are the change in mass of the secondary and primary star, respectively, and  $f_{trans}$  is the fraction of mass lost from the primary which does not accrete onto the secondary and is removed from the system. From Table 2, we see that the results depend only slightly on  $f_{trans}$  and for most of the simulations, we use  $f_{trans} = 0.5$ . During this phase, the loss of orbital angular momentum is determined by the parameterization of de Loore & De Greve (1992):

$$\frac{\Delta J_{orb}}{J_{orb}} = 1 - \left(1 - \frac{\Delta M_{tot}}{M_{tot}}\right)^\gamma, \quad (11)$$

where  $J_{orb}$  and  $M_{tot}$  are the pre-overflow values. The value of the parameter  $\gamma$  is poorly constrained. However, as seen in Table 2, uncertainty in  $\gamma$  has very little effect on the results. For most of the simulations, we use  $\gamma = 2.1$  as estimated by De Greve *et al.* (1985).

For common envelope evolution, we assume that no mass is gained by the secondary star and that the primary loses its hydrogen envelope. For the ratio of post-common envelope to pre-common envelope binary separation, we use Webbink (1984):

$$\frac{A_f}{A_i} = \frac{\alpha_{CE} r_L q}{2} \left( \frac{M_{He}}{(M_p - M_{He}) + \frac{1}{2} \alpha_{CE} r_L M_s} \right), \quad (12)$$

where  $r_L = R_L/A_i$  is the dimensionless Roche lobe radius of the primary (Eggleton 1983),

$$r_L = \frac{0.49q^{-2/3}}{0.6q^{-2/3} + \ln(1 + q^{-1/3})}. \quad (13)$$

$M_{He}$  is the mass of the primary’s helium core and  $\alpha_{CE}$  represents the efficiency with which orbital energy is injected into the common envelope. The fate of close binary systems depends strongly upon this parameter and the current set of hydrodynamical simulations (Taam & Bodenheimer 1991; Yorke, Taam & Bodenheimer 1995; Rasio & Livio 1996) do not yet provide a definitive value for this parameter. Indeed,  $\alpha_{CE}$  is probably a function of binary system.<sup>5</sup> However, as can be seen in Table 2, by choosing a higher efficiency, we increase the numbers for all the binary populations. In our comparison with observation, we use our simulations only to provide upper limits and, to be conservative, we maximize the numbers by choosing a high efficiency ( $\alpha_{CE} = 1$ ).

Although the parameter  $\alpha_{CE}$  has not yet been constrained by hydrodynamical simulations, conclusions can be drawn about specific aspects of common-envelope evolution. For example, Taam & Bodenheimer (1991) found that because He-star giants do not have the steep density profiles of the hydrogen counterparts, the likely outcome of a common-envelope phase with a He-star giant single star system in which the two stars have merged. In our code, these systems can no longer produce any of the massive X-ray binaries, but we retain the object for the pulsar velocities. However, as they make up less than 0.1% of the total number of binary systems, they have little effect on the pulsar velocity distribution.

The high density medium that surrounds neutron star in the common envelope phase cause neutrinos, rather than photons, to be the dominant coolant. Hence, the accretion rate onto the neutron star is not limited by the Eddington rate (Chevalier 1993,1996; Brown 1995; Fryer *et al.* 1996). For hydrogen giants, angular momentum (Chevalier 1996) or explosions induced by neutrino heating (Fryer *et al.* 1996) may restrict the accretion and allow the neutron star to survive this phase. However, in the denser environments of helium star giants, angular momentum and neutrino heating will not be sufficient to prevent black hole formation. In our simulations, we assume that neutron stars survive hydrogen-giant common envelope phases, but collapse to black holes if they progress through a helium-giant common envelope phases.

Mass loss due to stellar winds has a direct effect on stellar mass, which, in turn, has a strong effect upon the stellar radius. For both the models of Schaller *et al.* (1992) and those of Woosley, Langer & Weaver (1995), we parameterize the wind mass loss with

$$\Delta M_{wind} = f_{wind} \times \Delta M_{wind}^{models}, \tag{14}$$

where  $\Delta M_{wind}^{models}$  is the mass loss from the primary through its wind as predicted by Schaller *et al.* (1992), which agrees reasonably well with Woosley *et al.* (1995). The Schaller *et al.* mass-loss rates reflect upper limits to the mass-loss from winds and in our simulations, we consider the range  $0.0 < f_{wind} < 1.0$  (see Table 2). For most of our simulations,  $f_{wind}$  is set equal to unity.

### 3.3. Pulsar Velocities and Globular Clusters

An additional set of parameters can be derived if we include uncertainties in the galactic and globular cluster potential models. Distributing the pulsar formation position along spiral arms rather than a smooth disk may also have an effect on the simulated pulsar transverse-velocity distribution. For the purposes of this paper, we do not consider these effects. However, we do consider a range of globular cluster potentials from Drukier (1995) which lead to a range in retention fraction. Since the range in retention fraction

---

<sup>5</sup>Iben, Tutukov, & Yungelson (1996a) use a slightly different equation for the post-common to pre-common ratio in which the efficiency parameter  $\alpha_{CE}$  has a different meaning.

depends sensitively upon the kick distribution, we present these ranges separately for each kick distribution in §4.

#### 4. Natal Kick Distributions

Given a kick distribution, we can use our Monte Carlo code to derive the production rate of LMXBs, HMXBs, and DNSs as well as the pulsar velocity distribution and the globular cluster retention fraction. We stress that for all of the neutron-star populations, we overestimate the production rate. The ratio of our simulated rates to the actual rates may well be greater than ten (see §2). Similarly, our globular cluster retention fractions are upper limits. Recall that we normalize the simulated LMXB luminosity with the estimate of KW96 ( $L_{X,tot} = 1.7 \times 10^{39}$  ergs s<sup>-1</sup>), the HMXB population by the lower limit of Meurs & van den Heuvel (1989) ( $N = 28$  for  $L_X > 10^{36}$  ergs s<sup>-1</sup>), our DNS formation rate by  $10^{-6}$  yr<sup>-1</sup> (van den Heuvel 1995), and our derived retention fraction by 1% for the globular cluster NGC 6397 (Drukier 1995). We rule out only those pulsar velocity distributions whose Kolmogorov-Smirnov probability that the simulated and observed populations are derived from different parent populations is greater than 99%.

In §4.1 and 4.2, we present these ratios for a series of neutron-star kick distributions. Since we are calculating upper limits, we require that all ratios be greater than unity for a successful kick distribution. We use the results from §3 to create the best fit within the range of the many free binary-evolution parameters. Unless otherwise noted, we use the standard set of assumptions described in §3:  $\alpha_{IMF} = 2.7$ , mass limits =  $10, 40M_{\odot}$ ,  $\alpha_{MR} = 2.7$ ,  $q_0 = 0.35$ ,  $P(A_0) \propto 1/A_0$ ,  $P(e_0) = 1.0$ ,  $f_{trans} = 0.5$ ,  $\gamma = 2.1$ ,  $\alpha_{CE} = 1$ , and  $f_{wind} = 1.0$ .

In §4.2, we use the results from our series of  $\delta$ -function distributions to derive the neutron-star kick distribution which best fits all of the observations. We find that double-peaked kick distributions best fit both the pulsar velocity data and the binary system formation rates and we study these distributions in more detail. Our results depend most significantly on the distance measurements and we include a brief discussion of the effect of distance errors on our conclusions.

##### 4.1. Maxwellian and Flat Distributions

We ran a series of simulations with Maxwellian kick distributions for a variety of  $v_{rms}$ 's. Figure 8 summarizes the results of these simulations, using the standard input parameters. Table 3 gives the total number of bound neutron stars given the globular cluster models of Drukier (1995), along with the specific results for NGC 6397 and  $\omega$  Cen. The large kick velocities are required to explain the pulsar velocity distribution. Over 20% of the observed pulsars have transverse velocities greater than 500 km/s. Even without the effects of the galactic potential, high kick velocities are required to match the observations (Figure 4). We ran an alternate simulation using  $q_0 = 0.15$  and the mass limits =  $10, 100M_{\odot}$ . The lower value for  $q_0$  increases the number of LMXBs, while the higher mass limit allows more very massive stars to contribute to the HMXB and DNS populations. The results are summarized in Figure 9 and Table 4 and can be directly compared to Figure 8 and Table 3. For this simulation, we set the binary parameters to maximize the production rate of the neutron-star populations. Nevertheless, we see in Figure 9 that there is no acceptable solution. Keeping in mind that all of our ratios are upper limits, we conclude that it is impossible to fit the data with a Maxwellian kick distribution.

Similarly, we ran a series of simulations with flat kick distributions ranging from a magnitude of 0 km/s to a maximum of  $V_{max}$ . For these simulations, we used  $q_0 = 0.15$  and the standard parameter set. We see in Figure 10 and Table 5 that the fit is worse for this kick distribution than for a Maxwellian. Again, we conclude that it is impossible to fit the data with a flat kick distribution.

#### 4.2. Delta Function and Bimodal Distributions

We repeated this set of simulations once again for single delta function kick distributions. Figure 11 shows that we can find a delta function kick distribution that is consistent with the observed pulsar velocity distribution. However, the delta function kick distribution fails to explain our entire data set, especially the globular cluster retention fraction (Table 6). The best fit to the pulsar data gives a kick distribution with a velocity near 500-600 km/s, higher than the mean pulsar velocity. The mean kick must be higher due to the effects of binary evolution and the galactic potential which lower the mean neutron-star velocity after its initial kick. As mentioned in §2, the galactic potential can alter the pulsar velocities by up to 40% for some kick distributions.

Next, we use the results of the delta function simulations described above to infer a kick distribution that fits all observational constraints (LMXB, HMXB, DNS, globular cluster retention and the pulsar velocity distribution, which we bin into 5 roughly equal groups). To this effect, we approximate the kick velocity distribution by a weighted sum of individual delta functions of different kick magnitudes. We iterate on the weights until agreement between model and observations is reached.

In practice, the kick velocity distribution is approximated by the sum of 7 individual delta functions with equally spaced values ranging from 0 to 600 km/s. The observed pulsar velocity distribution fits into 5 bins having approximately equal number of objects (we slightly underestimate the true velocities here by lumping the very high velocities into one bin of pulsars with velocities greater than 500 km/s). Therefore, our system has 7 unknowns (the weights of the delta functions) and 9 constraints (3 binary systems, the globular cluster retention fraction, and 5 pulsar velocity bins). For each realization,  $\chi^2$  residuals are computed for each of the pulsar velocity bins and the best distribution is the one that minimizes these residuals while fitting all the constraints. The inclusion of additional delta function values did not lower the  $\chi^2$  residuals, so our 7 delta functions represent the kick distribution sufficiently given the current data. We varied the number of the bins of the observed pulsar velocity distribution as well as the binning procedure at fixed bin number and did not find any noticeable qualitative or quantitative change.

The best fit to the entire data set obtained from this procedure is illustrated in Fig. 12. Notice that the best fit distribution has a double-peaked profile<sup>6</sup>. This shape is required to explain all the observational constraints simultaneously. In other words, there must be a significant number of neutron stars born with very small kicks in order to explain the low velocity population (binaries and cluster members), while pulsar velocities indicate that another significant fraction must receive appreciable kicks. This trend can already be perceived in the raw data set; binary and galactic potential effects are not at the roots of this dichotomy. We have fit the same distribution without the binary and cluster member constraints (thick line in Figure 12) and find that the low-velocity ( $V_{kick} < 50$  km/s) population disappears.

To determine the robustness of this double-peaked distribution, we perform a number of tests. First, we

---

<sup>6</sup>The best fit is actually trimodal. However, we do not have sufficient data to mandate this trimodal distribution and a bimodal kick distribution fits within the constraints of the data. Occam’s razor limits us to a bimodal distribution at this time.

impose a lower limit to the weights of the intermediate bins (100 km/s - 400 km/s inclusive) and recompute the  $\chi^2$  residuals. We see from figure 12 that the distribution not only tries to keep its double-peaked profile, but the  $\chi^2$  residuals increase dramatically.

Second, to ascertain the effect of uncertainties in the radio pulsar distances on the double-peaked nature of the distribution, we artificially scale down the observed velocities, since an overestimate of the distance translates directly into an overestimation of the velocity. The  $\chi^2$  residuals for these best-fitting distributions are plotted in figure 13. If we reduce the distance estimate by 25%, the  $\chi^2$  residual for a flat kick distribution is only a factor of 5 times larger than our best-fitting double-peaked kick distribution. Thus, if there exists systematic errors in the distance measurements which overestimate the pulsar distances by over 25%, our conclusions requiring a double-peaked kick distribution will not hold.

We compare this double-peaked profile fit to our fits with the single-peak kick distributions by repeating the process used on the previous kick distributions. We again normalize the binary systems to calculate upper limits on their birthrates. For these simulations, we use  $q_0 = 0.15$  and the standard parameter set. The first series of simulations uses two  $\delta$ -function kick amplitudes. Roughly 30% are given a non-zero kick. We range this velocity from 500 to 950 km/s. Note in figure 14 that over this series of simulations, the kick distributions satisfy our minimum requirements for an allowed kick distribution. We also perform a second series of simulations using a kick distribution where 30% of the pulsars are given a kick of 0 km/s and the remaining 70% have a flat distribution with a mean of 625 km/s and a range in thickness (Figure 15). In both cases, the range of bound neutron stars in globular clusters is stable (28%-30%), corresponding to 2800 and 1000 neutron stars retained in NGC 6397 and  $\omega$  Cen, respectively.

## 5. Conclusions

We have created a Monte Carlo code which simulates the binary evolution of massive stellar systems and includes HMXB, LMXB, DNS, and radio pulsar phases. This code also follows the motions of these systems in the galactic potential. In addition, we calculate the retention fraction of neutron star systems in globular clusters. For this paper, we restricted our attention to the consequences of intrinsic kicks given to neutron stars at birth. First and foremost, a neutron star kick with a mean magnitude above 400 km/s is required to explain the pulsar velocity data for all the kick distributions we study. Figure 16 compares the observed transverse velocity data with the simulated transverse velocities for a Maxwellian kick distribution, a delta-function kick distribution and our double-peaked distribution (all with means above 400 km/s). The transverse velocities of a simulation without any neutron star kicks reveals the necessity of the kicks. Figure 16 also illustrates our claim that with the radio pulsar observations alone, low-number statistics prevents us from constraining the kick distribution, beyond simply requiring a kick. However, if we include the constraints placed upon the kick distribution from the binary populations and the globular cluster retention fraction, we can rule out many of the kick distributions appearing in the literature, including Maxwellian, flat, and  $\delta$ -function distributions (KW96, Brandt & Podsiadlowski 1995). Distributions which fit all of these constraints do exist, all of which are double-peaked. To explain the birthrates of the neutron star binary populations, we derive that roughly 30% of the neutron stars receive almost no kick. To explain the radio-pulsar velocity distribution, the remaining  $\sim 70\%$  receive a large kick (600 – 700 km/s).

Of course, there are many caveats to these conclusions. Our results depend sensitively upon the pulsar velocity distribution. If the pulsar distances and, hence, the velocities, are systematically lower by 25%,

a bimodal distribution is no longer necessary to explain the observations. However, it would require an extensive revision in the velocities to render some sort of neutron star kick unnecessary. Also, we rely heavily upon the reasonableness of binary population-synthesis models. Although we have studied the effects of many parameters and have calculated upper limits for all of our production rates, we can not eliminate the possibility that alternate models can explain the data. For instance, Iben & Tutukov (1996) explain the pulsar velocity distribution using the old distance model with no kick whatsoever by allowing only the highest-velocity neutron stars formed in binary evolution to become radio pulsars. Scrutiny of Figure 4 reveals that this is not possible unless we remove mass loss from winds or unless we ignore the results from hydrodynamical models and allow systems to survive common-envelope phases with He-stars. Even so, we require that only the fastest 1% of the neutron stars are observed as pulsars to explain the pulsar velocities from the old distance model. For the new distance model, this percentage becomes prohibitively small ( $\lesssim 0.1\%$ ). We incorporate the effects of a wide range in binary parameters, so that unless the understanding of binary population synthesis is drastically altered (winds, common envelope evolution, etc.), our basic conclusions still hold. In regimes where comparisons are possible, our results agree well with the models of KW96 and DS95.

This bimodal kick distribution has direct implications for a variety of objects whose evolution may involve a neutron star. To meet the isotropy requirements for gamma-ray bursts using accreting neutron stars in a galactic model. Podsiadlowski, Rees, & Ruderman (1995) require neutron star kicks upwards of 600 – 700 km/s. Our bimodal kick distribution results in  $\sim 70\%$  of the neutron star population with these velocities (Compare the post-binary evolution velocities in Figure 5). The bimodal distribution provides a natural break between the low-velocity neutron stars, which form X-ray binaries, and the high-velocity neutron stars which might make up the gamma-ray burst population in a galactic model (Leonard & Colgate 1994).

Our kick distribution can also be applied to explain O/B runaway stars. Although O/B runaway stars are not observed to be in close binaries, the observations do not preclude wide binary systems. (Gies & Bolton 1986, Sayer, Nice & Kaspi 1996, Philp *et al.* 1996). Figure 17 plots the distribution of velocities of O/B stars, both bound and unbound, assuming no neutron star kick. The unbound O/B stars are all moving slower than 50 km/s. The bound systems have significantly higher velocities, but very few O/B stars have velocities greater than 100 km/s. However, using our bimodal kick distribution, we see that unbound O/B stars can achieve velocities in excess of 200 km/s.

This bimodal distribution poses an additional problem for kick mechanisms. Not only must a kick mechanism produce neutron stars with velocities greater than 500 km/s, but the mechanism must be ineffective for a subset of the neutron star population. Since the submission of this paper, work by Cordes & Chernoff (1997) has appeared in the literature. This work concentrates upon an understanding of the biases of the pulsar velocity data and estimates of the pulsar ages. It predicts a double-peaked distribution of the *pulsar velocity distribution*, qualitatively agreeing with our results of the kick distribution. However, the quantitative differences make it clear that much more work must be done to gain a definitive answer on kick velocities.

Our simulations can be seen as the first step in constraining the natal neutron-star kick distribution. Although the double-peaked nature of the kick distribution is required by our calculations, there remains a wealth of observational data which can be used to constrain the quantitative nature and individual structure of the peaks. The orbital characteristics of the binary systems formed using a variety of kick distributions may also provide insight into the specifics of the distribution. For instance, wide-orbit LMXBs (KW96) and short-period DNSs (Fryer & Kalogera 1997) may further constrain the kick distribution. We have not yet

explored variations in the galactic potential and the scale-height distributions of the various neutron star systems. With improved distances and with an increasing sample of radio pulsars, we hope to apply this technique not just to constrain the neutron star kick and binary evolution, but also the galactic potential.

It is a pleasure to thank Vicky Kalogera for many helpful discussions on binary population synthesis and comments on the manuscript. We are grateful to Chad Engelbracht for many helpful discussions which clarified much of the paper. Paul Harding also provided useful advice on galaxy dynamics and stellar populations. We would also like to thank an the referee, Rachel Dewey, for many helpful comments and suggestions which improved the paper immensely. The work of C.F. and W.B. was partially supported by NSF grant AST 9206738 and a “Profil 2” grant from the Swiss National Science Foundation. A.B. acknowledges support from NSF grant AST 9217322.

## REFERENCES

- Anderson, S.B., Gorham, P.W., Kulkarni, S.R., Prince, T.A., & Wolszczan, A., 1990, *Nature*, 346, 42
- Bailyn, C.D. & Grindlay, J.E., 1990, *ApJ*, 353, 159
- Benz, W., Fryer, C.L., Herant, M., Colgate, S.A., in preparation
- Bhattacharya, D. & van den Heuvel, E.P.J., 1991, *Phys. Rev. Let.*, 203, 1
- Blaauw, A. 1961, *Bull. Astron. Inst. Neth.*, 505, 265
- Brandt, N. & Podsiadlowski, P., 1995, *MNRAS*, 274, 461
- Brown, G.E., 1995, *ApJ*, 440, 270
- Burrows, A. & Hayes, J., 1996, *Phys. Rev. Let.*, 76, 352
- Burrows, A. & Woosley, S.E., 1986, *ApJ*, 308, 680
- Caraveo, P., 1993, *ApJ*, 415, L111
- Chevalier, R.A., 1993, *ApJ*, 411, L33
- Chevalier, R.A., 1996, *ApJ*, 459, 322
- Colgate, S.A., & Leonard, P.J.T., 1993, *BATSE Gamma Ray Burst Workshop*
- Cordes, J.M., Romani, R.W., Lundgren, S.C., 1993, *Nature*, 362, 133
- Cordes, J.M., & Chernoff, D.F., *astro-ph/9707308*
- Curran, S.J., & Lorimer, D.R., 1995, *MNRAS*, 276, 347
- Dalton, W.W. & Sarazin, C.L., 1995, *ApJ*, 448, 369 (DS95)
- Davies, M.B. & Benz, W., 1995, *MNRAS*, 276, 876
- De Greve, J.P., Packet, W., De Landtsheer, A.C., 1985, *A&A* 290, 185
- De Loore, C., De Greve, J.P., 1992, *A&AS* 94, 453



- Dewey, R.J. & Cordes, J., 1987, *ApJ*, 321, 780
- Drukier, G.A., 1996, *MNRAS*, 280, 498
- Eggleton, P.P., 1983, *ApJ*, 268, 386
- Eggleton, P.P., & Verbunt, F., 1986, *MNRAS*, 220, 13P
- Flannery, B.P., & van den Heuvel, E.P.J., 1975, *A&A*, 39, 61
- Frail, D.A., Goss, W.M., & Whiteoak, J.B.Z., 1994, *ApJ*, 342, 260
- Fryer, C.L., Benz, W., Herant, M., 1996, *ApJ*, 460, 801
- Fryer, C.L., Benz, w., Herant, M., Colgate, S.A., submitted to *ApJ*
- Fryer, C.L., & Kalogera, V., accepted by *ApJ*
- Gaensler, B.M, & Johnston, S., 1995, *MNRAS*, 273, L73
- Garmany, C.D., Conti, P.S., Massey, P., 1980, *ApJ*, 242, 1063
- Gies, D.R. & Bolton, C.T., 1986, *ApJS*, 61, 419
- Gunn, J.E., & Ostriker, J.E., 1970, *ApJ*, 160, 979
- Habets, G.M.H.J., 1985, Ph.D. Thesis, University of Amsterdam
- Hansen, B., & Phinney, S., 1997, accepted by *MNRAS*
- Hogeveen, S.J., 1991, Ph.D. Thesis, University of Amsterdam
- Iben, I. Jr. & Tutukov, A.V., 1996, *ApJ*, 456, 738
- Iben, I. Jr., Tutukov, A.V., & Yungelson, L.R., 1995, *ApJS*, 100, 217
- Iben, I. Jr., Tutukov, A.V., & Yungelson, L.R., 1995, *ApJS*, 100, 233
- Johnston, S., Koribalski, B., Weisberg, J.M., Wilson, W., 1996, *MNRAS*, 279, 661
- Kalogera, V., 1996, accepted by *ApJ*
- Kalogera, V. & Webbink, R.F., 1996a (KW96) submitted to *ApJ*
- Kalogera, V. & Webbink, R.F., 1996b, *ApJ*, 458, 301
- Kaspi, V.M., Bailes, M., Manchester, R.N., Stappers, B.W., Bell, J.F., 1996, *Nature*, 381, 584
- Kirshner, R.P., Morse, J.A., Winkler, P.F., & Blair, J.P., 1989, *ApJ*, 342, 260
- Kraicheva, Z.T., Popova, E.I., Tututukov, A.V., Yungelson, L.R., 1979, *SvA*, 56, 520
- Lamb, D.Q., 1995, *PASP*, 107, 1152
- Leonard, P.J.T., 1990, *JRASC*, 84, 216
- Leonard, P.J.T., 1995, *MNRAS*, 277, 1080

- Leonard, P.J.T. & Dewey, R.J., 1992, Conf. on Luminous High-Latitude Stars
- Lorimer, D.R., Lyne, A.G., & Anderson B., 1995, MNRAS, 275, L16
- Lyne, A.G., Lorimer, D.R., 1994, Nature, 369, 127L
- Meurs, E.J.A. & van den Heuvel, E.P.J., 1989, A&A, 226, 88
- Mihalas, D., & Binney, J., 1968, Galactic Astronomy, Chapter 4, W.H. Freeman & Co.
- Miyamoto, M. & Nagai, R., 1975, PASJ, 27, 533
- Morse, J.A., Winkler, P.F., & Kirshner, R.P., 1995, AJ, 109, 2104
- Narayan, R., & Ostriker, J.P., 1990, ApJ, 352, 222
- Nomoto, K., Kondo, Y., 1991, ApJ, 367, L19
- Philp, C.J., Evans, C.R., Leonard, P.J.T., Frail, D.A., 1996, AJ, 111, 1220
- Podsiadlowski, P., Rees, M.J., Ruderman, M., 1995, MNRAS, 273, 755
- Rasio, F.A., & Livio, M., 1996, submitted to ApJ
- Sayer, R.W., Nice, D.J., & Kaspi, V.M., 1996, ApJ, 461, 357
- Scalo, J. M. 1986, Fund. of Cosmic Phys., 11, 1
- Schaller, G., Schaerer, D., Meynet, G., Maeder, A., 1992, A&AS, 98, 523
- Taam, R.E., & Bodenheimer, P., 1995, ApJ, 451, 308
- Yorke, H.W., Taam, R.E., & Bodenheimer, P., 1995, ApJ, 451, 308
- Tammann, G.A., Loeffler, W., Schroeder, A., 1994, ApJS, 92, 487
- Taylor, J.H. & Cordes, J.M., 1993, ApJ, 411 674
- Taylor, J.H., Manchester, R.N., & Lyne, A.G., 1993, ApJS, 88, 529
- Tutukov, A.V., Chugai, N.N., & Yungelson, L.R., 1984, Pisma v Ast. Zh., 10, 586
- van den Heuvel, E.P.J., 1983, Accretion-Driven Stellar X-ray Sources, Cambridge University Press
- van den Heuvel, E.P.J., 1995, JApA, 16, 255
- van den Heuvel, E.P.J., & Lorimer, D.R., 1996, MNRAS, 283, L37
- van den Heuvel, E.P.J., & Rappaport, S., 1986, Physics of Be stars, Proc. of the 92nd IAU Coll., 291, Cambridge University Press
- Wasserman, I., Cordes, J., & Chernoff, D., 1997, in preparation
- Webbink, R.F., 1979, ApJ, 227, 178
- Webbink, R.F., 1984, ApJ, 277, 355

Woosley, S.E. & Baron, E., 1992, ApJ, 391, 228

Woosley, S.E., Langer, N., Weaver, T.A., 1995, ApJ, 411, 823

Woosley, S.E., Langer, N., Weaver, T.A., 1995, ApJ, 448, 315

Yamaoka, H., Shigeyama, T., Nomoto, K., 1993, ApJ, 267, 433

Table 1. Parameters: Initial Conditions<sup>a</sup>

	LMXB $10^{39}$ erg $s^{-1}$	HMXB N with $L_X > 10^{36}$ erg $s^{-1}$	DNS Rate ( $10^{-6}y^{-1}$ )
$V_{kick} = 0 \text{ km s}^{-1}$			
“standard”	2.80	92.7	45.2
$\alpha_{IMF} = 2.1$	2.62	142.4	62.7
$M_{min,max} = 8, 40$	1.36	65.8	26.0
$M_{min,max} = 10, 100$	1.68	47.7	36.1
$\alpha_{MR} = 1.0^b$	0.227	60.9	200.
$\alpha_{MR} = 0.0^b$	2.41	82.6	135.
$\alpha_{MR} = 2.7, q_0 = 0.15^c$	11.1	152.1	26.8
$P(e) = \delta(e)$	2.91	71.2	54.6
$A_{max} = 10^6$	1.26	48.2	73.4
$V_{kick} = 200 \text{ km s}^{-1}$			
“standard”	4.16	40.3	1.15
$\alpha_{IMF} = 2.1$	4.47	53.3	1.42
$M_{min,max} = 8, 40$	2.81	35.5	0.641
$M_{min,max} = 10, 100$	2.56	29.4	0.820
$\alpha_{MR} = 1.0$	0.420	35.1	3.56
$\alpha_{MR} = 0.0$	3.07	42.3	2.49
$\alpha_{MR} = 2.7, q_0 = .15$	19.3	100.5	0.751
$P(e) = \delta(e)$	5.12	32.8	1.11
$A_{max} = 10^6$	1.71	21.8	0.547
$V_{kick} = 400 \text{ km s}^{-1}$			
“standard”	1.68	13.0	0.474
$\alpha_{IMF} = 2.1$	1.98	16.9	0.656
$M_{min,max} = 8, 40$	1.24	10.7	0.289
$M_{min,max} = 10, 100$	0.937	10.5	0.384
$\alpha_{MR} = 1.0$	0.159	10.6	1.85
$\alpha_{MR} = 2.7, q_0 = 0.35$	1.68	13.0	0.474
$\alpha_{MR} = 2.7, q_0 = .15$	6.95	29.8	0.437
$P(e) = \delta(e)$	1.96	10.7	0.491
$A_{max} = 10^6$	0.660	7.51	0.265

<sup>a</sup>For these simulations, we use a “standard” set of parameters:  $\alpha_{IMF} = 2.7$ , mass limits =  $10, 40M_{\odot}$ ,  $\alpha_{MR} = 2.7$ ,  $q_0 = 0.35$ ,  $P(A_0) \propto 1/A_0$ ,  $P(e_0) = 1.0$ ,  $f_{trans} = 0.5$ ,  $\gamma = 2.1$ ,  $\alpha_{CE} = 1$ , and  $f_{wind} = 1.0$ . We have combined the simulations with a SN rate =  $0.01y^{-1}$  and a binary fraction determined by the choice of mass ratio (unless otherwise stated, we use 0.35). We use the technique in §2 to determine each population.

<sup>b</sup>For  $\alpha_{MR} = 1.0, 0.0$ , we assume a binary fraction of 0.43.

<sup>c</sup>For  $\alpha_{MR} = 2.7$ ,  $q_0 = 0.15$ , we assume a binary fraction of 0.65.

Table 2. Parameters: Binary Evolution<sup>a</sup>

	LMXB 10 <sup>39</sup> erg s <sup>-1</sup>	HMXB N with $L_X > 10^{36}$ erg s <sup>-1</sup>	DNS Rate (10 <sup>-6</sup> y <sup>-1</sup> )
$V_{kick} = 0 \text{ km s}^{-1}$			
“standard”	2.80	92.7	45.2
$f_{trans} = 0.1$	2.47	60.3	45.0
$f_{trans} = 0.9$	2.39	61.9	36.0
$\alpha_{CE} = 0.2$	$\lesssim 0.028$	4.82	45.2
$\alpha_{CE} = 2.0$	4.94	181.5	45.3
$f_{wind} = 0$	1.75	89.7	39.2
$\gamma = 1.5$	2.48	238.2	36.3
$V_{kick} = 200 \text{ km s}^{-1}$			
“standard”	4.16	40.3	1.15
$f_{trans} = 0.1$	4.06	23.3	2.00
$f_{trans} = 0.9$	4.43	32.0	0.955
$\alpha_{CE} = 0.2$	$\lesssim 0.028$	2.28	0.0232
$\alpha_{CE} = 2.0$	11.4	71.7	2.13
$f_{wind} = 0$	24.2	65.0	6.01
$\gamma = 1.5$	4.71	85.9	1.38
$V_{kick} = 400 \text{ km s}^{-1}$			
“standard”	1.68	13.0	0.474
$f_{trans} = 0.1$	1.54	6.94	0.854
$f_{trans} = 0.9$	1.71	9.93	0.513
$\alpha_{CE} = 0.2$	$\lesssim 0.028$	0.839	0.00664
$\alpha_{CE} = 2.0$	3.7	20.4	0.927
$f_{wind} = 0$	13.3	21.3	2.43
$\gamma = 1.5$	1.45	29.3	0.577

<sup>a</sup>For these simulations, we use a “standard” set of parameters:  $\alpha_{IMF} = 2.7$ , mass limits = 10, 40 $M_{\odot}$ ,  $\alpha_{MR} = 2.7$ ,  $q_0 = 0.35$ ,  $P(A_0) \propto 1/A_0$ ,  $P(e_0) = 1.0$ ,  $f_{trans} = 0.5$ ,  $\gamma = 2.1$ ,  $\alpha_{CE} = 1$ , and  $f_{wind} = 1.0$ . We have combined the simulations with a SN rate = 0.01y<sup>-1</sup> and a binary fraction determined by the choice of mass ratio (unless otherwise stated, we use 0.35). We use the technique in §2 to determine each population.

Table 3. NS Retention: Maxwellian Kick Distribution:  $q_0 = 0.35^a$

$(v_{rms}^2)^{1/2}$ (km s <sup>-1</sup> )	Range in RF <sup>b</sup>	RF	NS retained NGC6397	RF	NS retained $\omega$ Cen
0.0	91.6 – 99.9%	98%	$9.5 \times 10^3$	99.1%	$3.5 \times 10^3$
50.0	4.71 – 49.0%	15.4%	$1.5 \times 10^3$	29.2%	$1.0 \times 10^3$
100.0	1.91 – 38.3%	5.30%	$5.1 \times 10^2$	11.1%	$3.9 \times 10^2$
150.0	1.19 – 37.5%	2.95%	$2.9 \times 10^2$	5.83%	$2.0 \times 10^2$
200.0	0.88 – 18.9%	2.06%	$2.0 \times 10^2$	3.88%	$1.4 \times 10^2$
250.0	0.70 – 13.6%	1.60%	$1.6 \times 10^2$	2.89%	$1.0 \times 10^2$
300.0	0.57 – 10.2%	1.27%	$1.2 \times 10^2$	2.26%	79
350.0	0.49 – 8.1%	1.08%	$1.0 \times 10^2$	1.90%	67
400.0	0.42 – 6.6%	0.93%	90	1.63%	57
450.0	0.38 – 5.5%	0.83%	81	1.42%	49
500.0	0.34 – 4.7%	0.74%	72	1.28%	46
550.0	0.31 – 4.1%	0.66%	64	1.12%	37
600.0	0.29 – 3.6%	0.61%	59	1.02%	35

<sup>a</sup>Standard Parameters:  $\alpha_{IMF} = 2.7$ , mass limits = 10,  $40M_{\odot}$ ,  $\alpha_{MR} = 2.7$ ,  $q_0 = 0.35$ ,  $P(A_0) \propto 1/A_0$ ,  $P(e_0) = 1.0$ ,  $f_{trans} = 0.5$ ,  $\gamma = 2.1$ ,  $\alpha_{CE} = 1$ , and  $f_{wind} = 1.0$ .

<sup>b</sup>The range in retention fractions (RF) is determined using the Fokker-Planck models of Drukier (1995).

Table 4. NS Retention: Maxwellian Kick Distribution:  $q_0 = 0.15^a$

$(v_{rms}^2)^{1/2}$ (km s <sup>-1</sup> )	Range in RF	RF	NS retained NGC6397	RF	NS retained $\omega$ Cen
0.0	89.0 – 99.7%	95%	$9.2 \times 10^3$	97%	$3.4 \times 10^3$
50.0	3.96 – 70.4%	18.4%	$1.8 \times 10^3$	39.6%	$1.4 \times 10^3$
100.0	1.25 – 54.7%	4.8%	$4.7 \times 10^2$	12.7%	$4.4 \times 10^2$
150.0	0.70 – 37.5%	2.25%	$2.2 \times 10^2$	5.65%	$2.0 \times 10^2$
200.0	0.50 – 25.0%	1.41%	$1.4 \times 10^2$	3.26%	$1.2 \times 10^2$
250.0	0.41 – 17.0%	1.04%	$1.0 \times 10^2$	2.21%	77
300.0	0.31 – 12.1%	0.77%	75	1.59%	56
350.0	0.28 – 8.9%	0.67%	65	1.3%	46
400.0	0.23 – 6.9%	0.55%	53	1.1%	37
450.0	0.21 – 5.4%	0.47%	46	0.89%	31
500.0	0.19 – 4.4%	0.44%	43	0.80%	28
550.0	0.18 – 3.7%	0.39%	38	0.69%	24
600.0	0.17 – 2.4%	0.34%	33	0.61%	21

<sup>a</sup>same as table 3,  $q_0 = 0.15$ .

Table 5. NS Retention: Flat Kick Distribution<sup>a</sup>

<i>MeanVelocity</i> (km s <sup>-1</sup> )	Range in RF <sup>b</sup>	RF	NS retained NGC6397	RF	NS retained $\omega$ Cen
50.0	9.44 – 69.9%	20.1%	$1.9 \times 10^3$	33.3%	$1.2 \times 10^3$
150.0	3.13 – 32.1%	6.66%	646	11.0%	385
200.0	2.35 – 24.1%	5.00%	485	8.28%	290
250.0	1.88 – 19.2%	3.99%	387	6.62%	232
300.0	1.56 – 16.0%	3.33%	323	5.52%	193
350.0	1.34 – 13.7%	2.85%	276	4.73%	166

<sup>a</sup>Parameters:  $\alpha_{IMF} = 2.7$ , mass limits = 10,  $40M_{\odot}$ ,  $\alpha_{MR} = 2.7$ ,  $q_0 = 0.15$ ,  $P(A_0) \propto 1/A_0$ ,  $P(e_0) = \delta(e_0)$ ,  $f_{trans} = 0.5$ ,  $\gamma = 2.1$ ,  $\alpha_{CE} = 1$ , and  $f_{wind} = 1.0$ .

<sup>b</sup>The range in retention fractions (RF) is determined using the Fokker-Planck models of Drukier (1995).

Table 6. NS Retention:  $\delta$ -Function Kick Distribution<sup>a</sup>

<i>Velocity</i> (km s <sup>-1</sup> )	Range in RF <sup>b</sup>	RF	NS retained NGC6397	RF	NS retained $\omega$ Cen
0.0	89.5 – 99.9%	97.1%	$9.4 \times 10^3$	98.7%	$3.5 \times 10^3$
50.0	0.19 – 96.8%	3.62%	$3.5 \times 10^2$	42.5%	$1.5 \times 10^3$
100.0	.011 – 67.3%	0.077%	7	0.398%	13.9
150.0	$4.2 \times 10^{-3}$ – 36.6%	0.033%	3	0.127%	4
200.0	$2.8 \times 10^{-3}$ – 11.8%	0.028%	3	0.078%	3
250.0	$1.2 \times 10^{-3}$ – 1.39%	0.016%	2	0.045%	2
300.0	$5.1 \times 10^{-4}$ – 0.43%	$7.6 \times 10^{-3}\%$	1	0.025%	1
350.0	$2.2 \times 10^{-5}$ – 0.30%	$5.5 \times 10^{-3}\%$	1	0.021%	1
400.0	$1.7 \times 10^{-6}$ – 0.21%	$2.1 \times 10^{-3}\%$	0	0.011%	0
450.0	0.0 – 0.16%	$1.0 \times 10^{-3}\%$	0	$7.9 \times 10^{-3}\%$	0
500.0	0.0 – 0.11%	$7.1 \times 10^{-4}\%$	0	$4.7 \times 10^{-3}\%$	0
550.0	0.0 – 0.080%	$1.7 \times 10^{-4}\%$	0	$2.3 \times 10^{-3}\%$	0
600.0	0.0 – 0.062%	$7.9 \times 10^{-5}\%$	0	$1.4 \times 10^{-3}\%$	0
650.0	0.0 – 0.023%	$5.1 \times 10^{-6}\%$	0	$2.5 \times 10^{-4}\%$	0

<sup>a</sup>Standard Parameters:  $\alpha_{IMF} = 2.7$ , mass limits = 10,  $40M_{\odot}$ ,  $\alpha_{MR} = 2.7$ ,  $q_0 = 0.35$ ,  $P(A_0) \propto 1/A_0$ ,  $P(e_0) = 1.0$ ,  $f_{trans} = 0.5$ ,  $\gamma = 2.1$ ,  $\alpha_{CE} = 1$ , and  $f_{wind} = 1.0$ .

<sup>b</sup>The range in retention fractions (RF) is determined using the Fokker-Planck models of Drukier (1995).



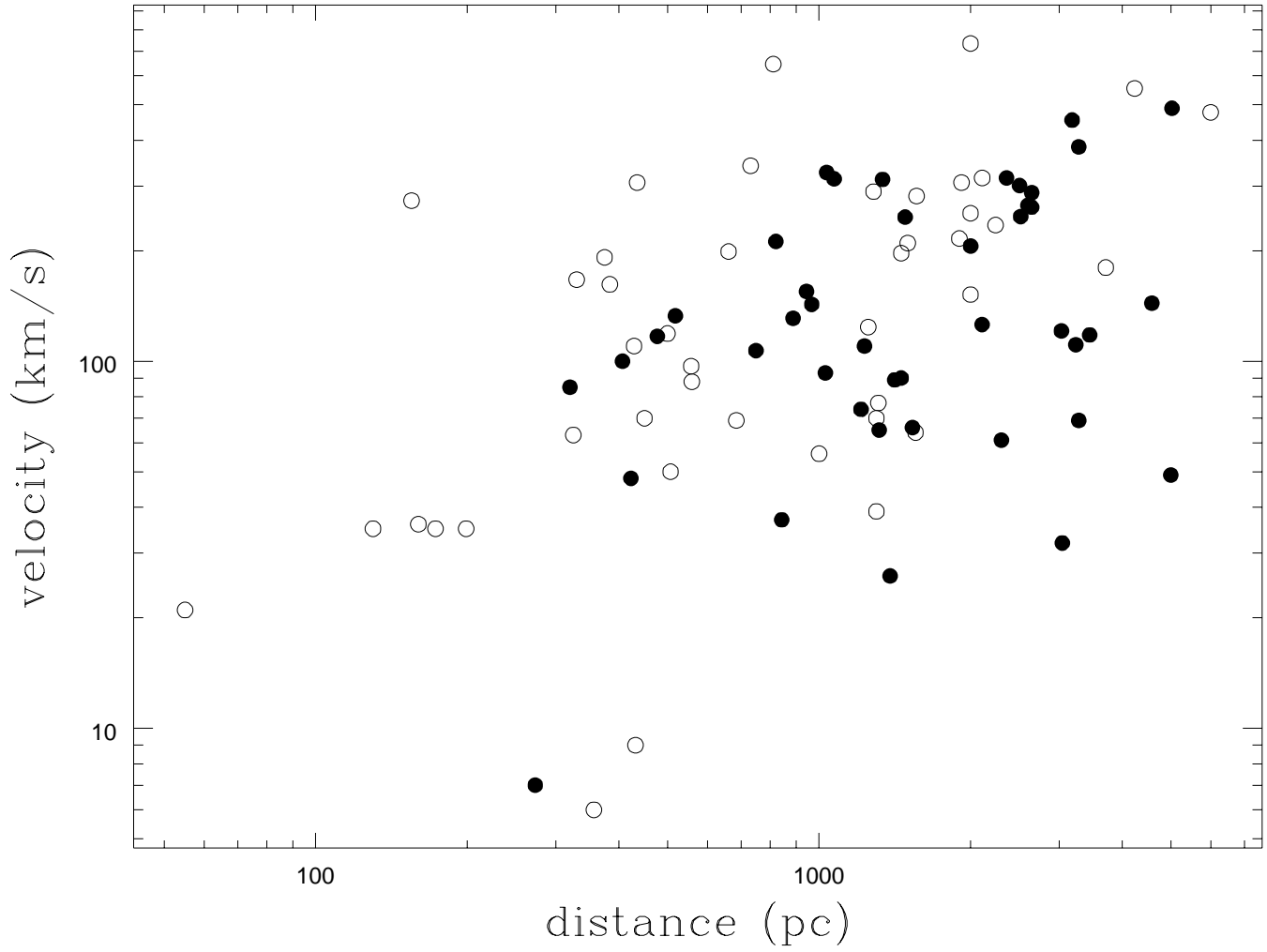


Fig. 1.— The observed transverse velocities of radio pulsars versus their distances  $D$  from the Sun (Harrison *et al.* 1993). The open circles denote the 44 pulsars with proper motions determined by Harrison *et al.* and the filled circles are the 43 additional pulsars with proper motions calculated by other techniques.

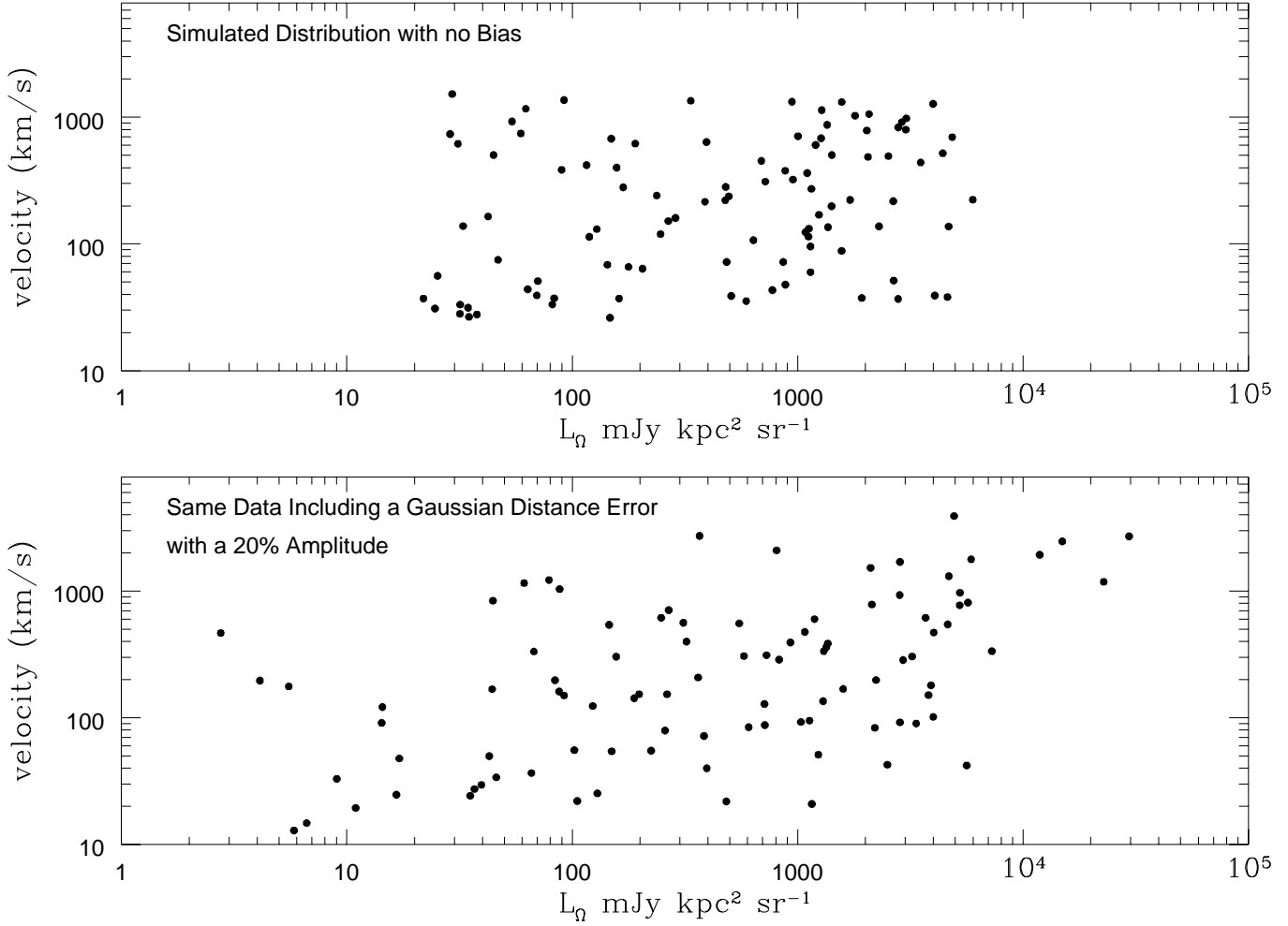


Fig. 2.— Luminosity versus velocity for a simulated sample (no biases) without distance errors on the left and with distance errors on the right. The pulsars in the simulated sample are evenly chosen in velocity/luminosity space with no intrinsic biases. We assume the distance errors are Gaussian with a magnitude of 20% distance (Taylor & Cordes 1993 assume gaussian distance errors on the order of 10%). The higher-velocity pulsars *appear* to be more luminous.

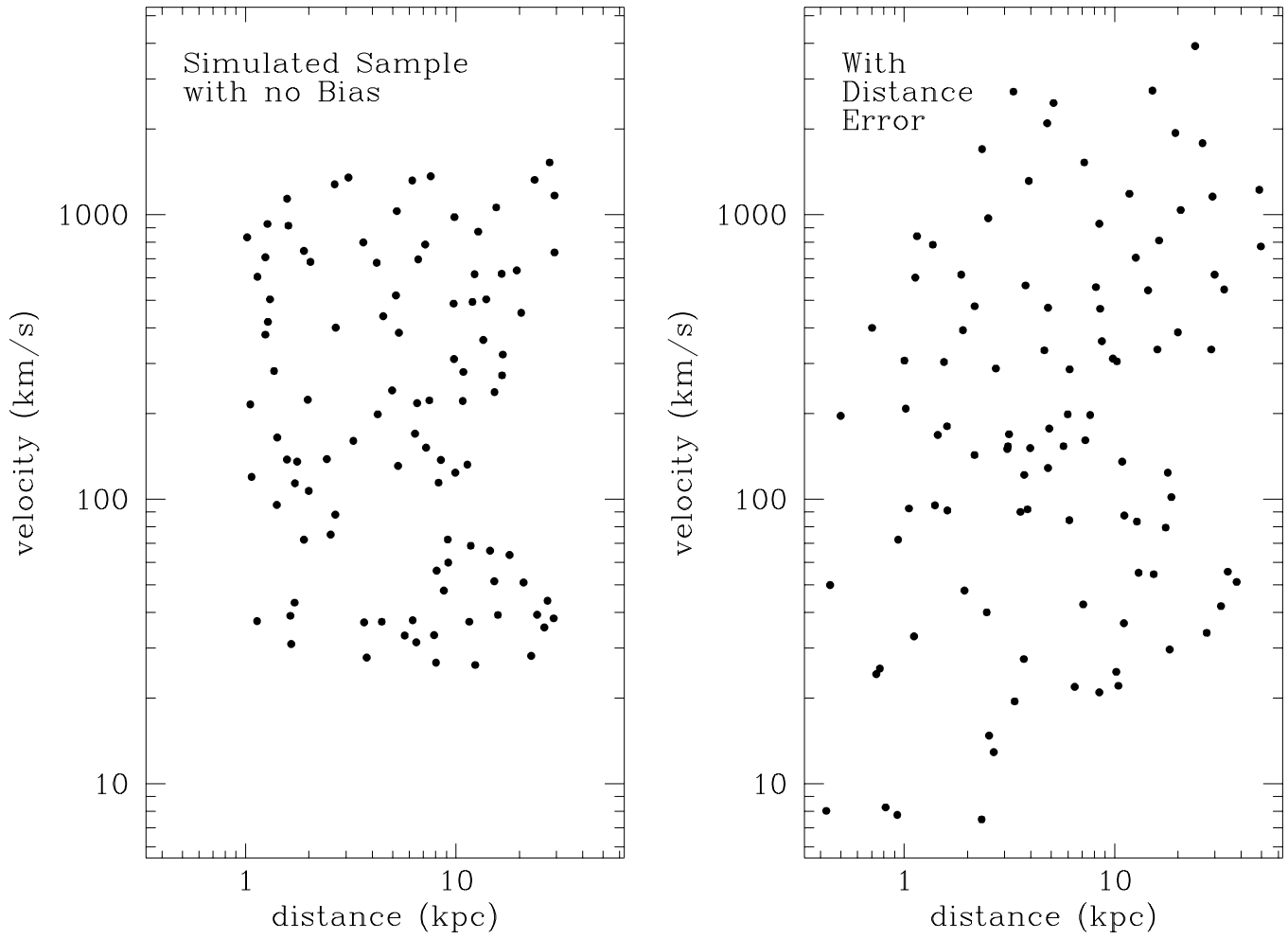


Fig. 3.— The same as Figure 2, except velocity is plotted versus distance. Note that with distance errors, another fictitious bias appears with the nearby pulsars tending to have lower velocities.

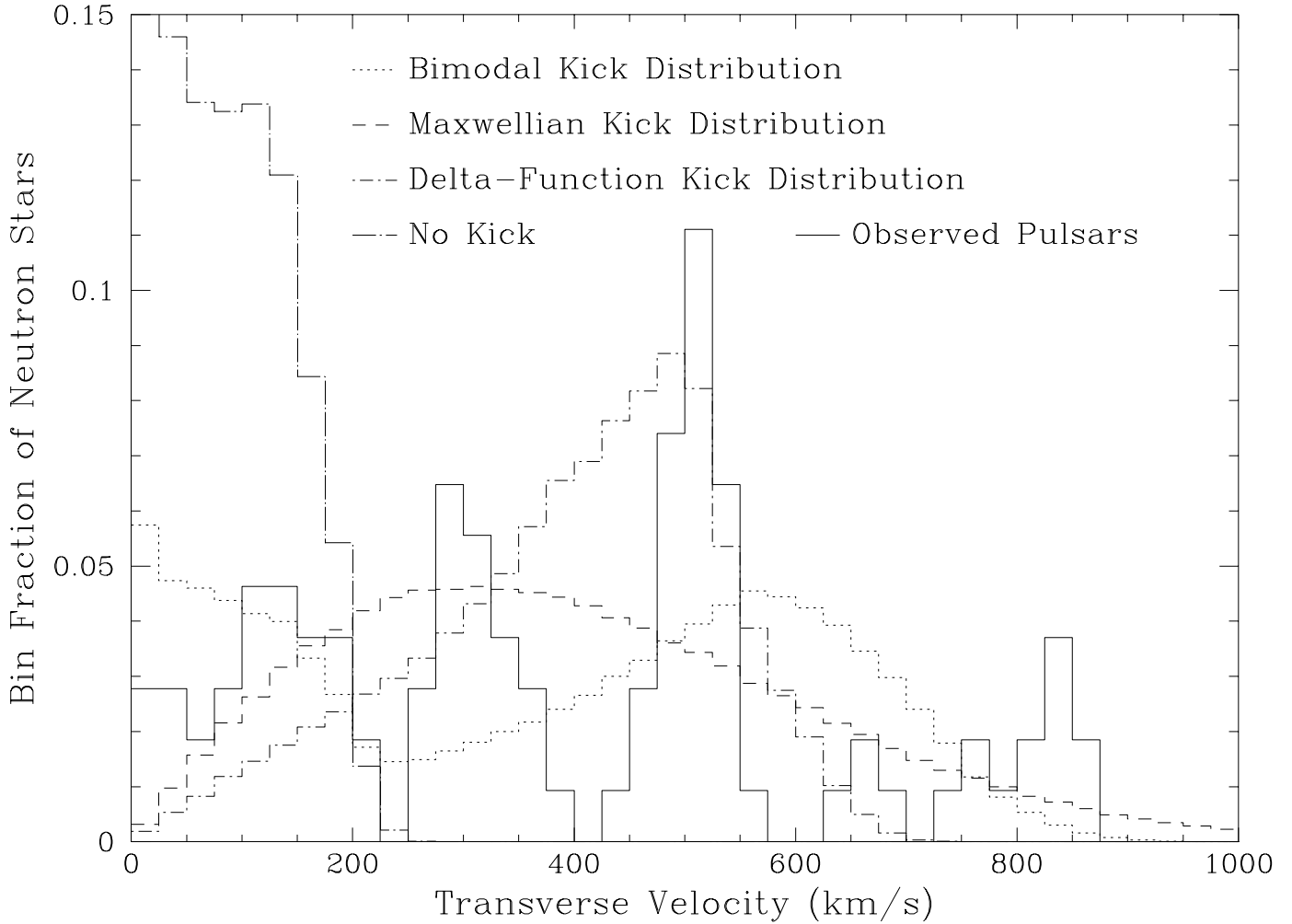


Fig. 4.— Transverse velocity distributions for the best fitting double-peaked, Maxwellian, and delta-function kick distributions along with a smoothed (within the quoted errors - Taylor, Manchester, & Lyne 1993) distribution of the observed pulsar transverse velocities. Included for comparison is the transverse velocity distribution for a simulation with no natal neutron star kick. The simulation with no neutron star kicks clearly does not fit the data, but the other distributions can not be ruled out with such small number statistics.

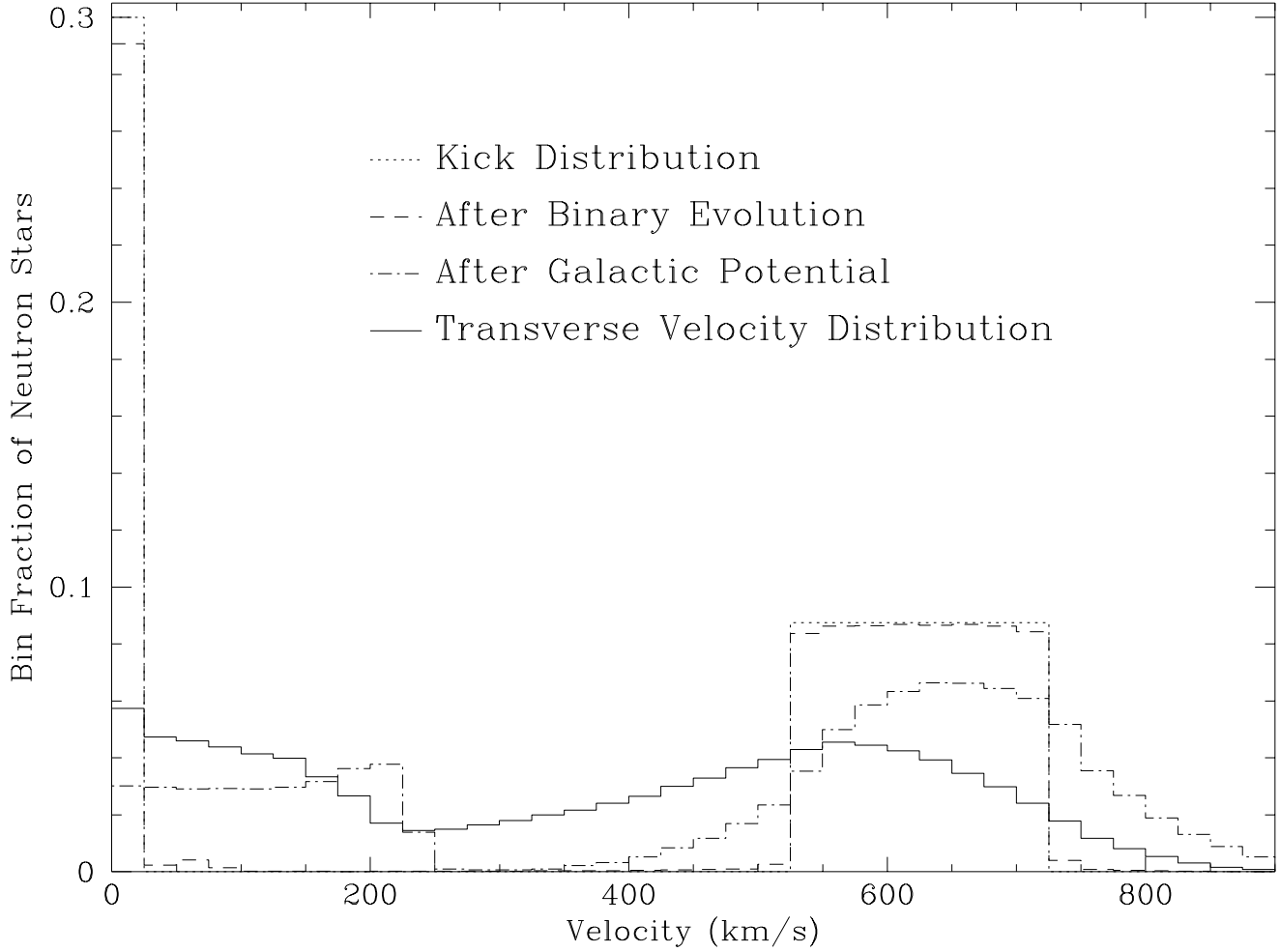


Fig. 5.— The dependence of the pulsar velocity distribution for a double-peaked kick distribution (dotted curve) on binary evolution (dashed curve) and the galactic potential (dot-dashed curve). The solid curve gives the pulsar transverse-velocity distribution which is then compared to the observations. Note that the transverse velocity distribution bears little resemblance to its parent kick distribution, illustrating the importance of including the effects of binary evolution and motion in the galaxy in extracting the actual kick distribution from the observations.

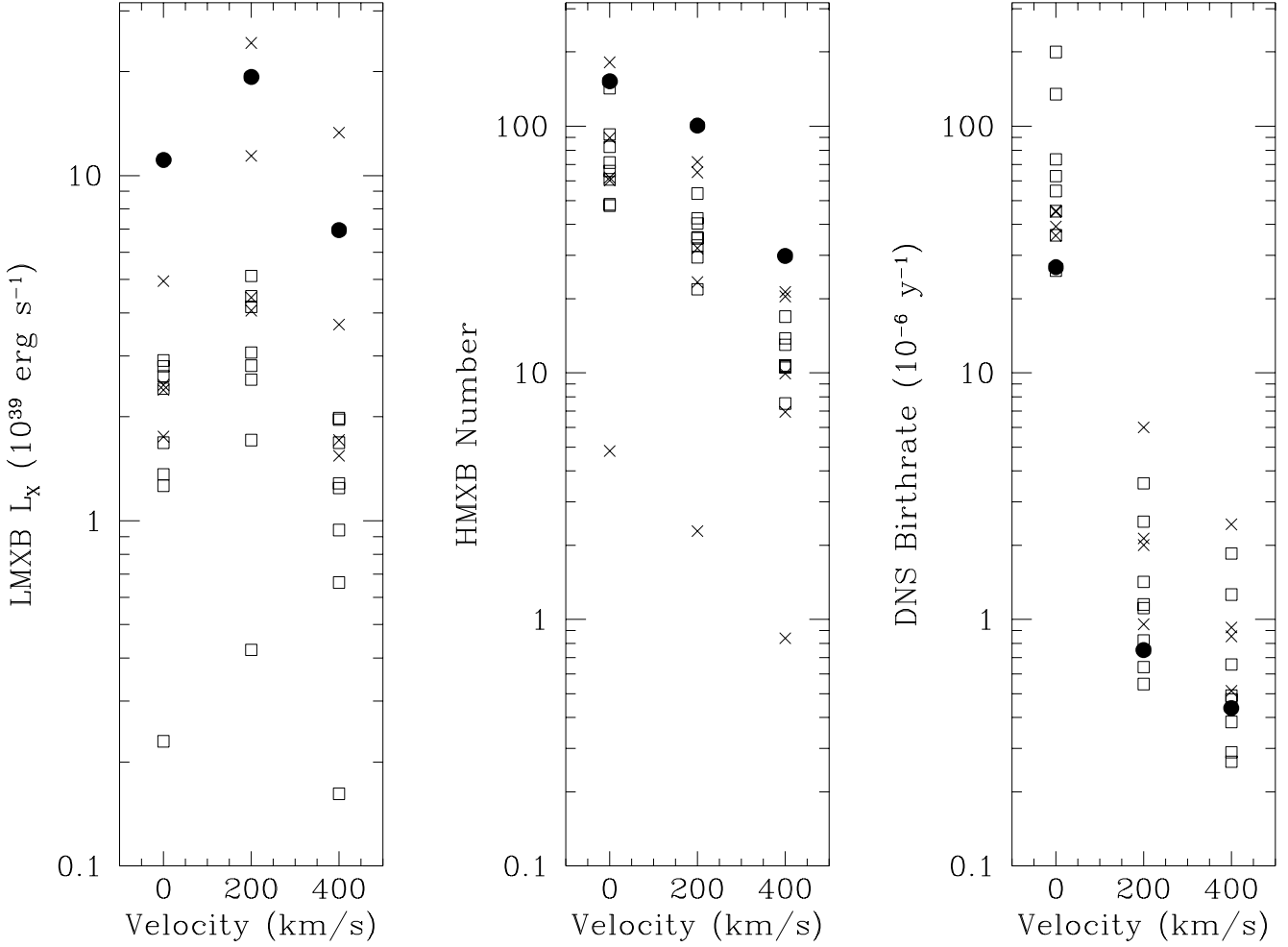


Fig. 6.— The dependence of the various neutron star binaries with respect to the various initial binary and evolutionary parameters and velocity. The filled circles correspond to the standard parameter set. The open squares correspond to the initial binary parameters (§3.1) and the crosses correspond to the binary evolution parameters (§3.2).

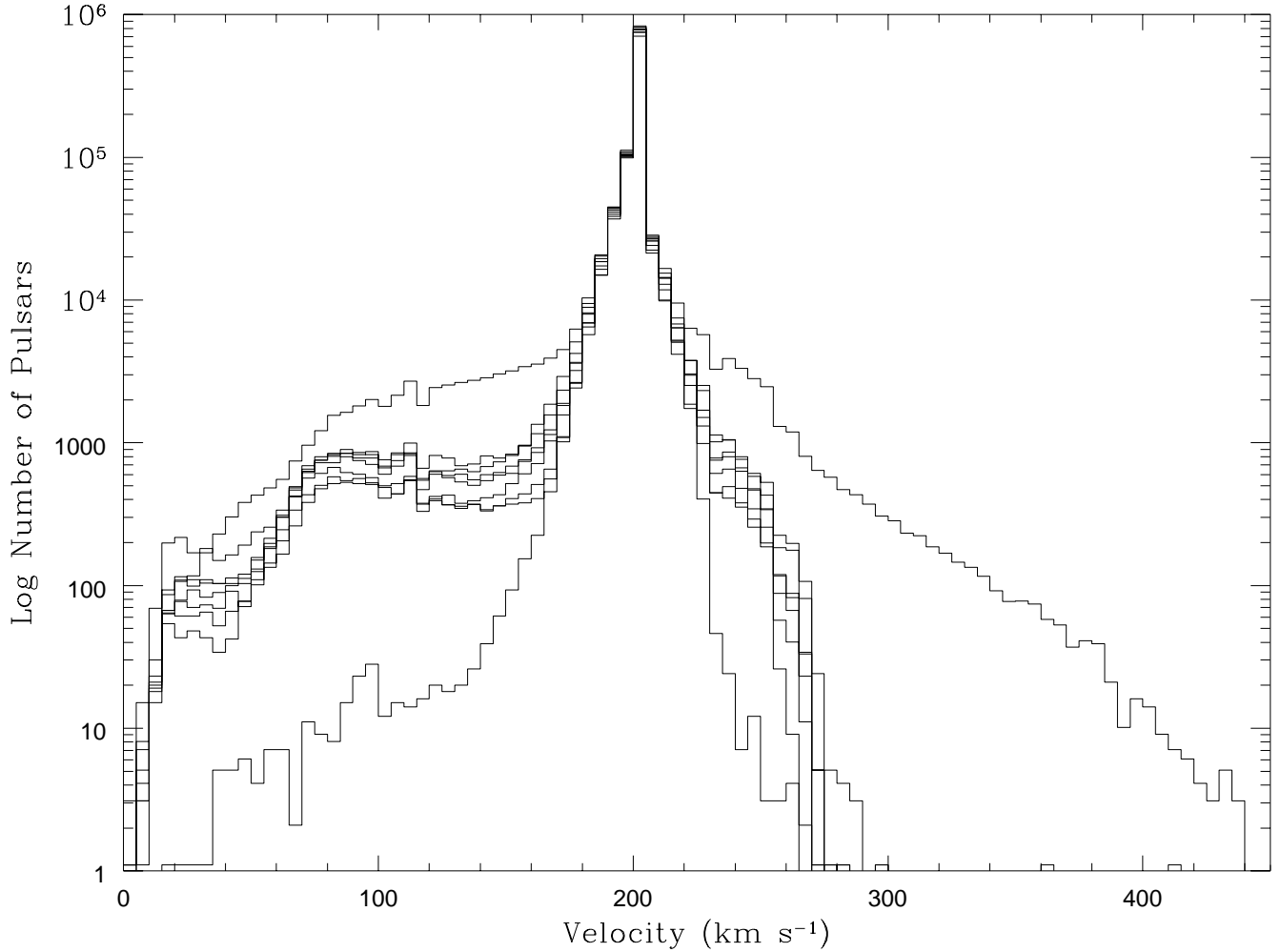


Fig. 7.— The three-dimensional velocity distribution of pulsars for a range of initial and binary-evolution parameters with a  $\delta$ -function kick of 200 km/s. The binary parameters affect only a small number of the pulsars. The typical pulsar velocity is unchanged by even extreme changes in the binary parameters. The largest differences come from assuming that there is no mass lost from winds which allows very tight pre-SN systems to form and leads to the broadest profile. The narrow profile is the velocity distribution calculated by setting  $\alpha_{CE} = 0.2$  which prevents the formation of these close binaries. Note, however, that the bulk of the binary parameters have little effect on the pulsar velocity distribution.

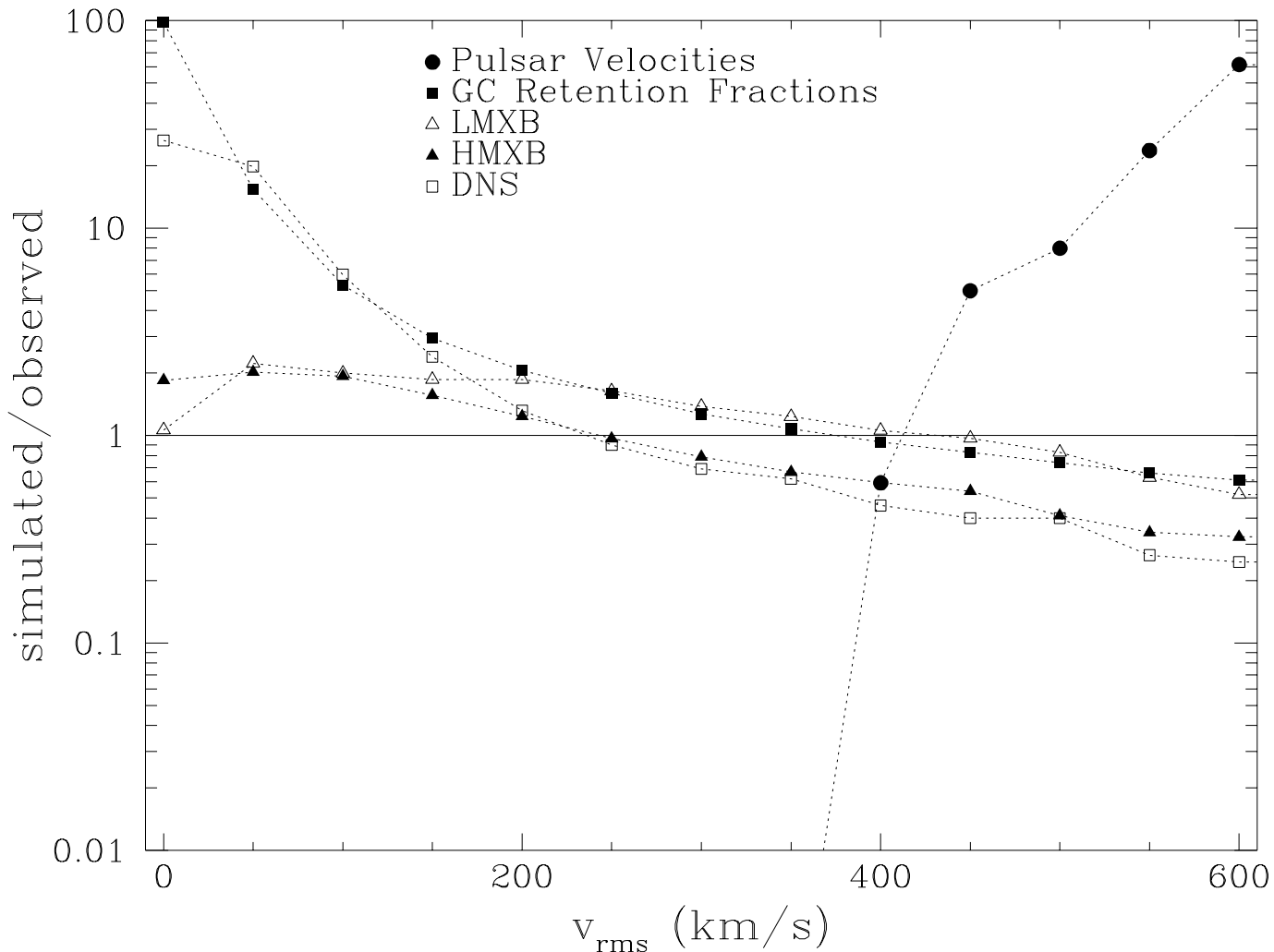


Fig. 8.— The simulated populations normalized by the observations versus the root-mean-square velocity for a Maxwellian Distribution. For the pulsars, we plot  $(99.99 - P)$  where  $P$  is the percentage probability that the simulated velocity distribution and the observed velocity distribution are not from the same parent population. We use our standard set of binary parameters. A “successful” solution is one for which all the normalized numbers are greater than unity simultaneously.



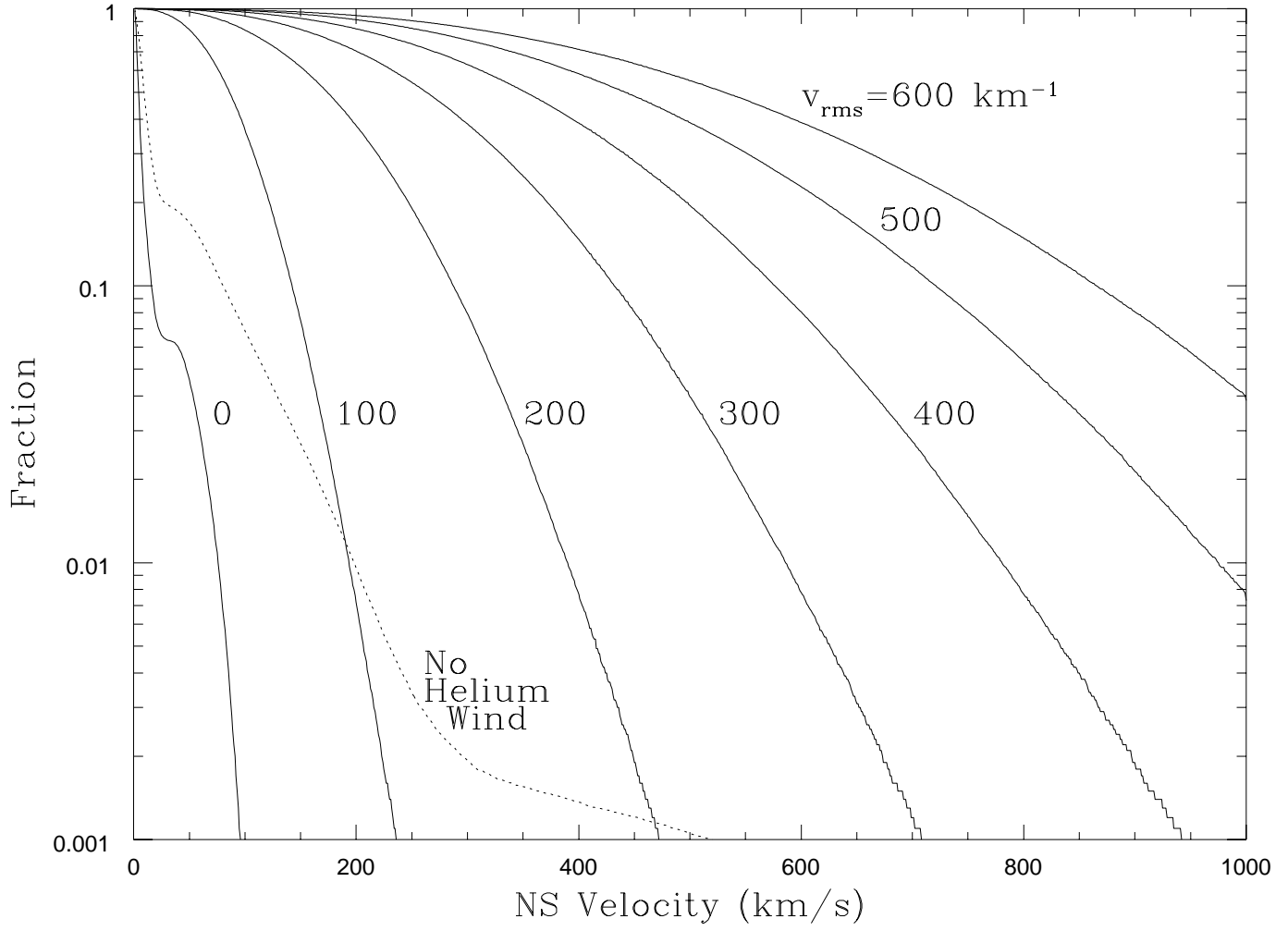


Fig. 9.— Fraction of Neutron Stars with a velocity greater than a given velocity versus that velocity for the series of Maxwellian kick distributions. The dotted line that shows a zero kick simulation with no mass loss from He winds is included to demonstrate how binary effects can change the velocity distribution.

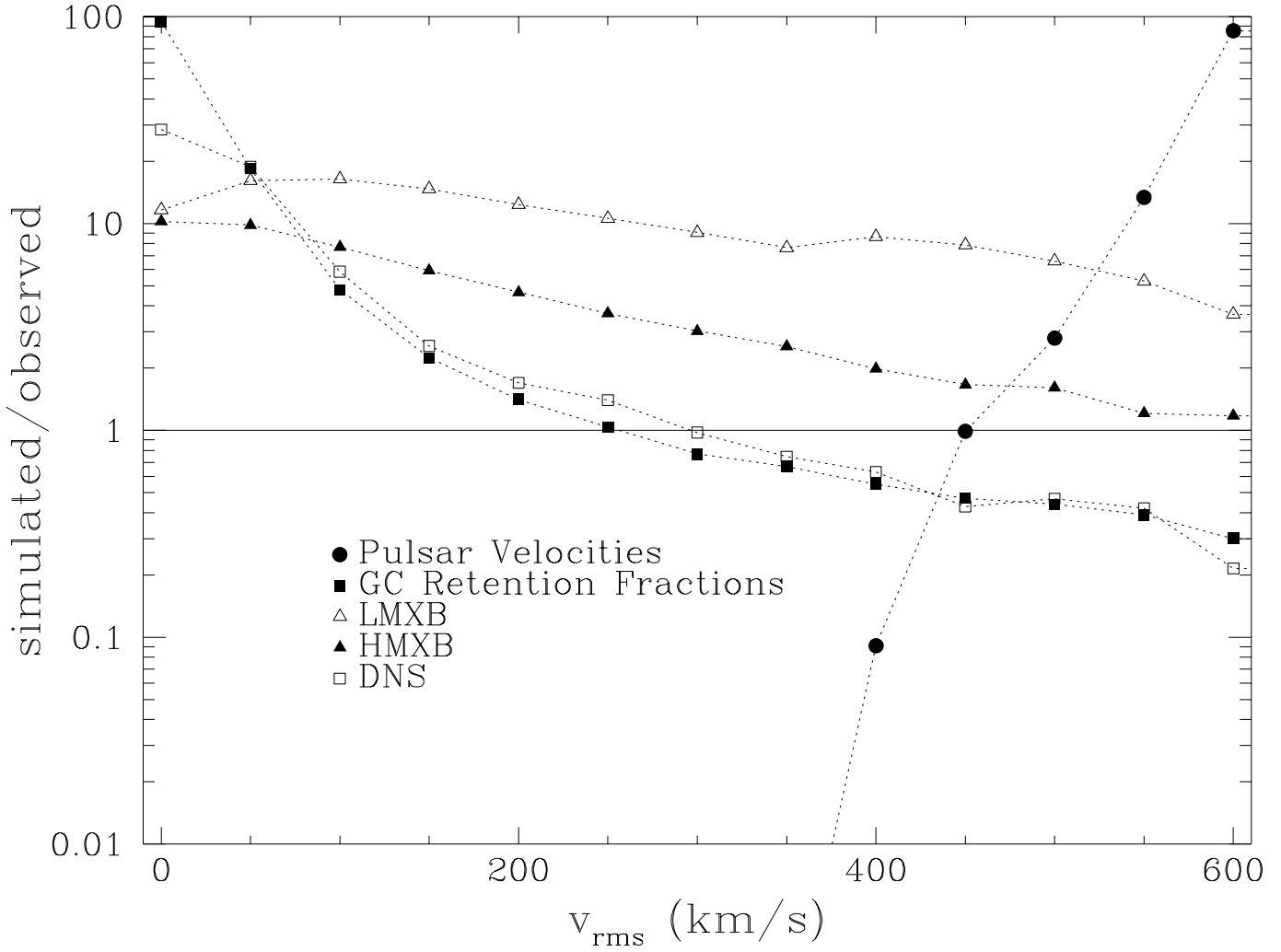


Fig. 10.— The same as Fig. 8, but with  $q_0 = 0.15$  and  $M_{l,u} = 10, 100 M_{\odot}$ .

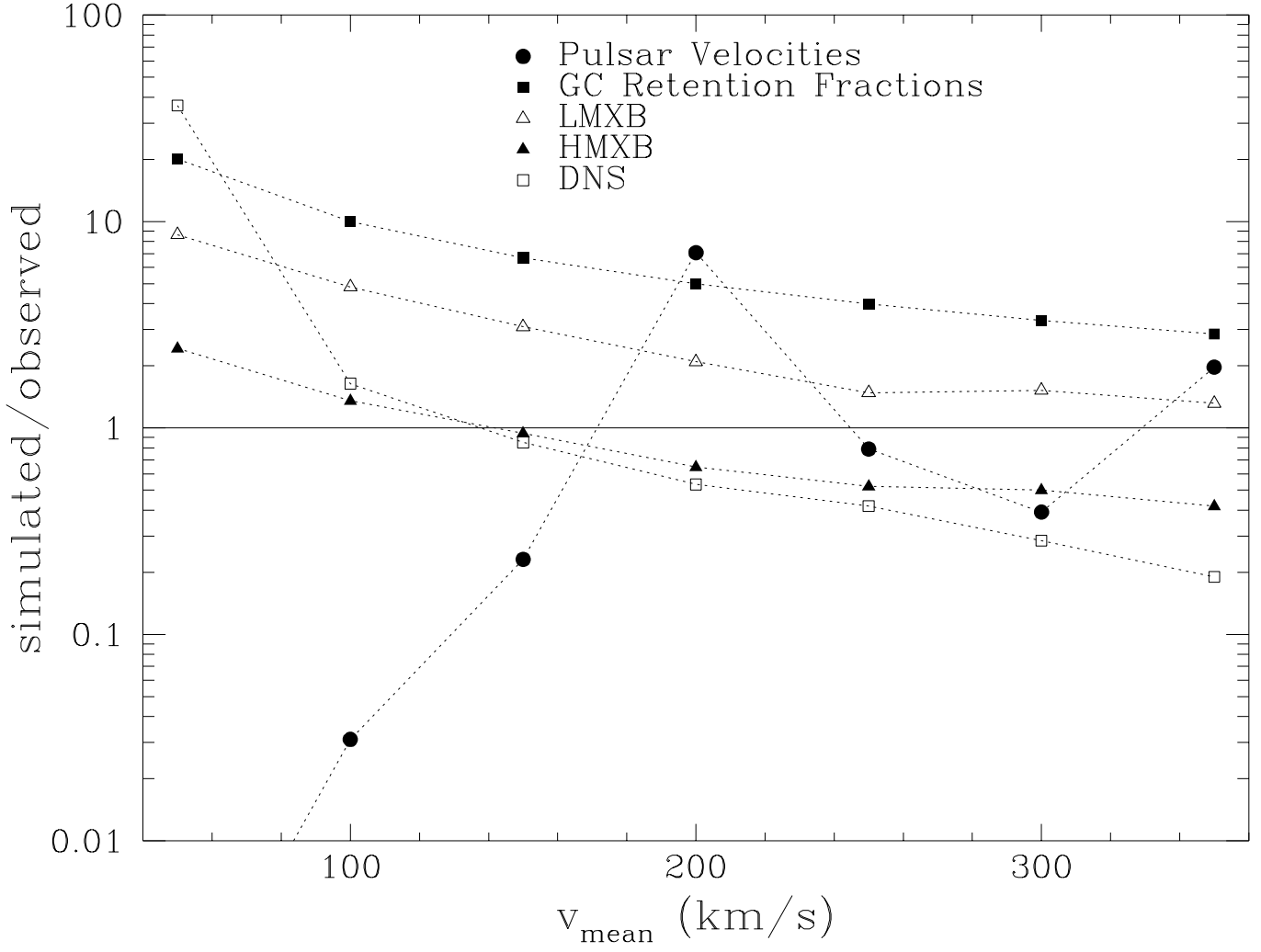


Fig. 11.— The same as Fig. 8, but for flat kick distributions with  $q_0 = 0.15$ .

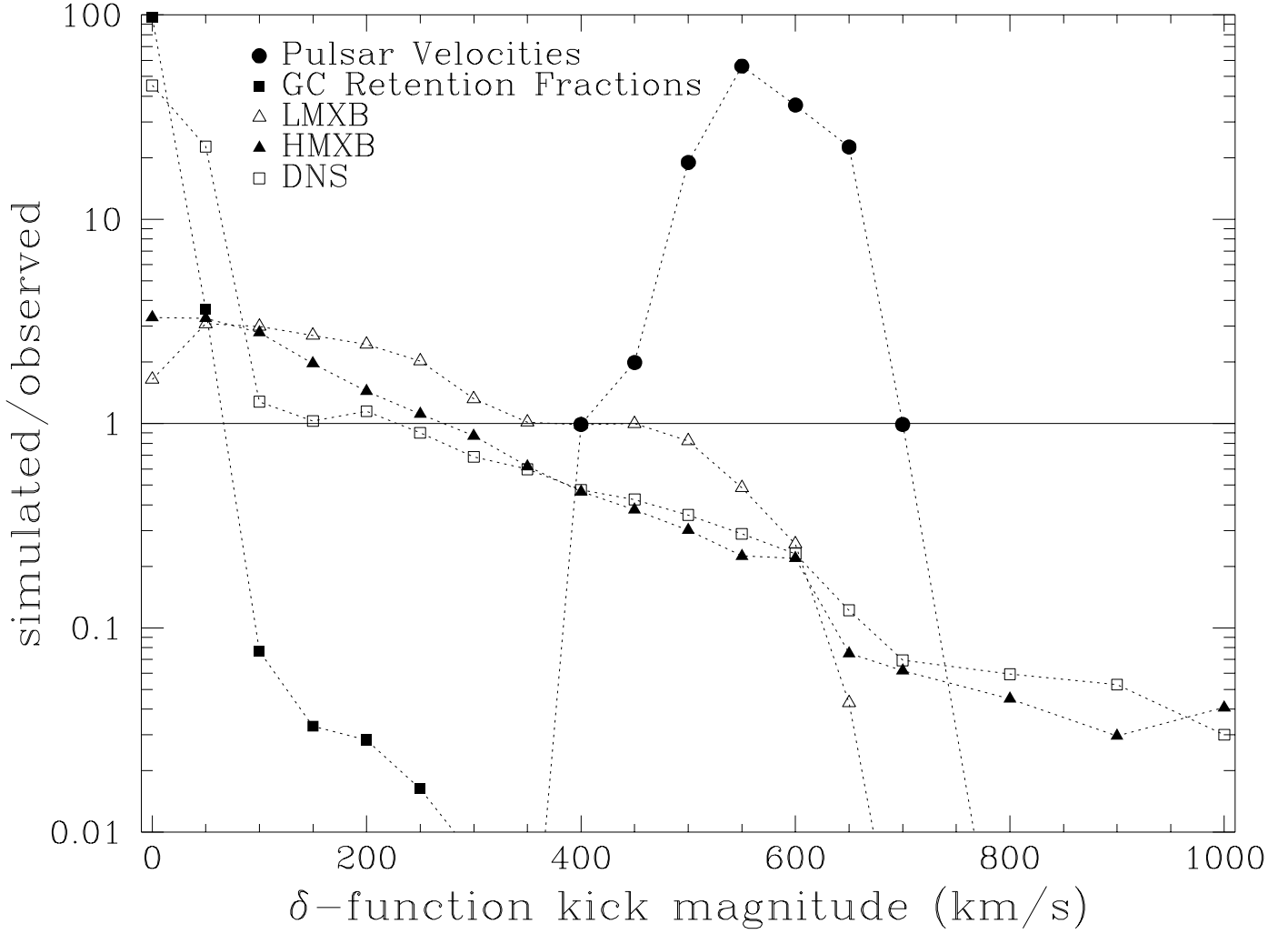


Fig. 12.— The same as Fig. 8, but for  $\delta$ -function kicks.

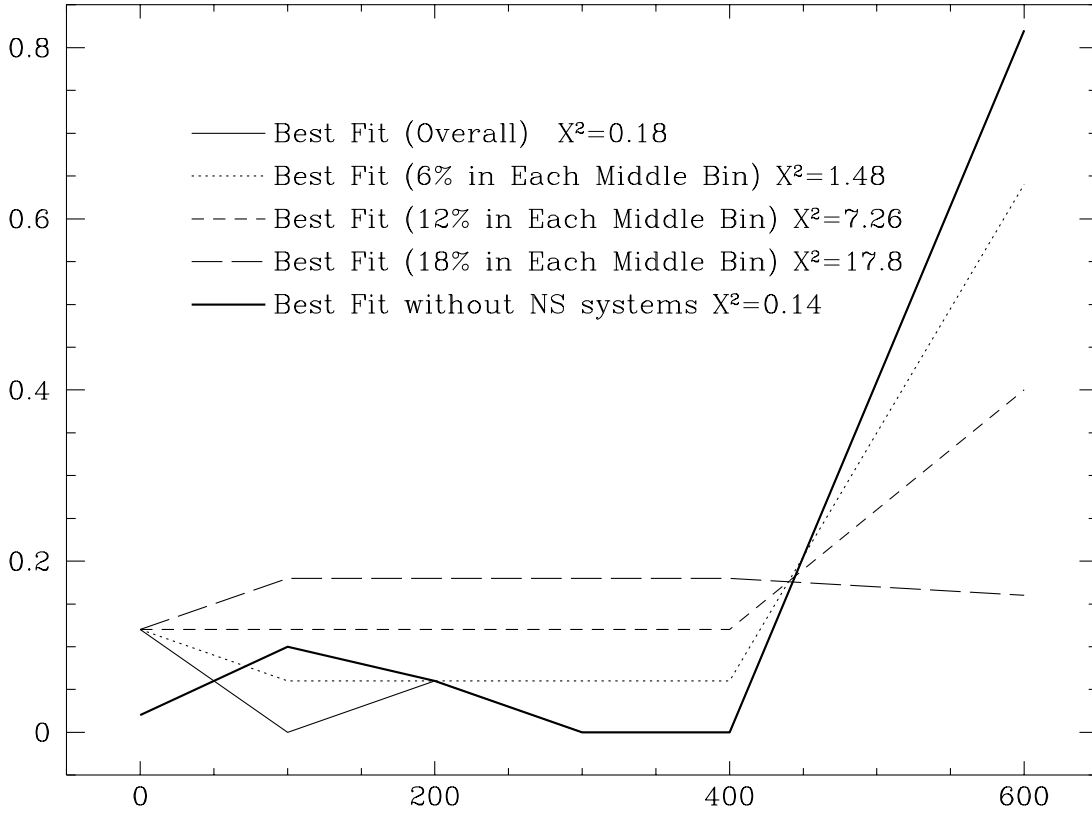


Fig. 13.— Kick distributions with fraction of neutron stars versus velocity bin. The solid line denotes the best-fitting overall kick profile. The remaining curves are constrained by requiring that the middle range of velocities be non-zero to varying degrees.

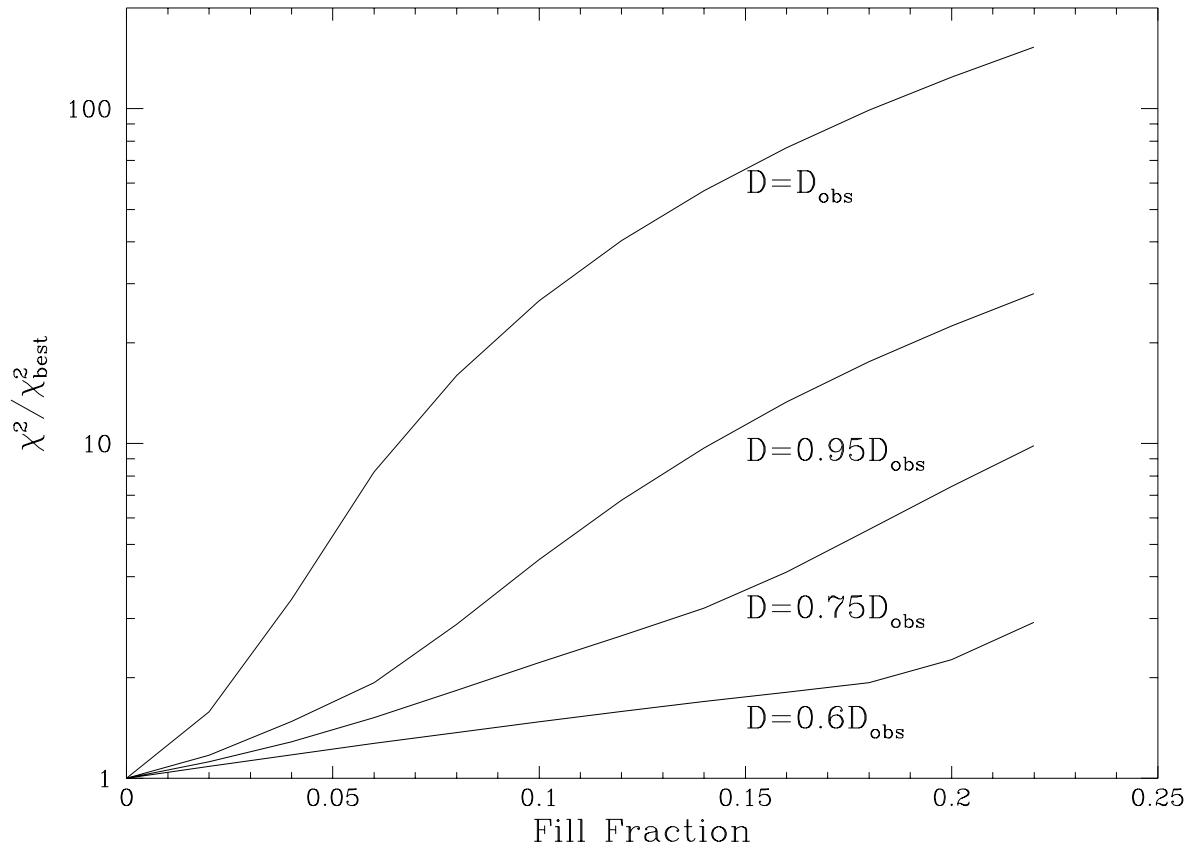


Fig. 14.—  $\chi^2$  residuals versus the degree to which the middle velocities are filled, normalized by the residuals from the best-fitting overall distribution. The curves represent a range of scale factors for the distance.

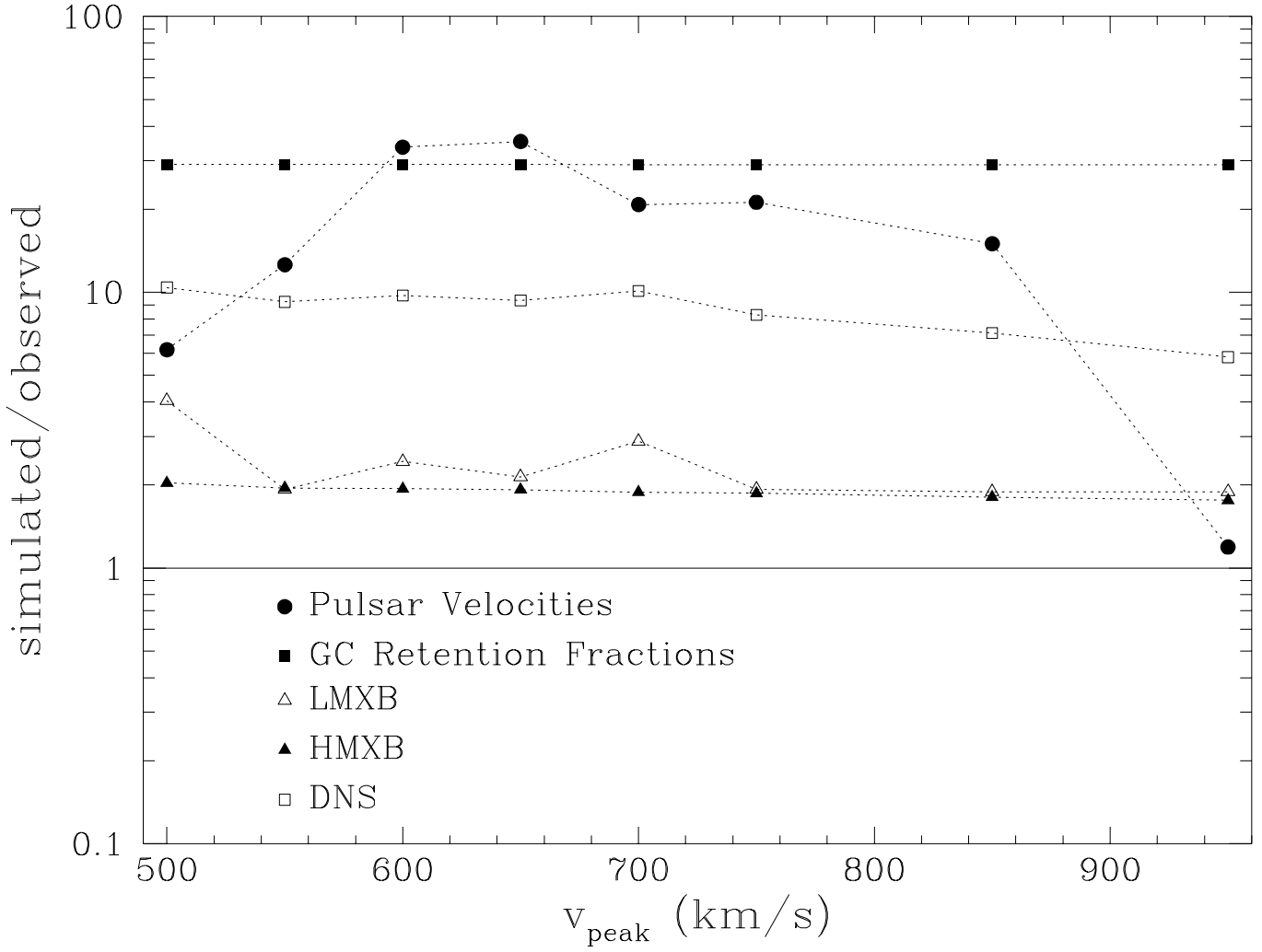


Fig. 15.— Same as Fig 8. with a double-peaked  $\delta$ -function distribution: 30% at 0 km/s and 70% at the value on the plot. Again, we use  $q_0 = 0.15$ .

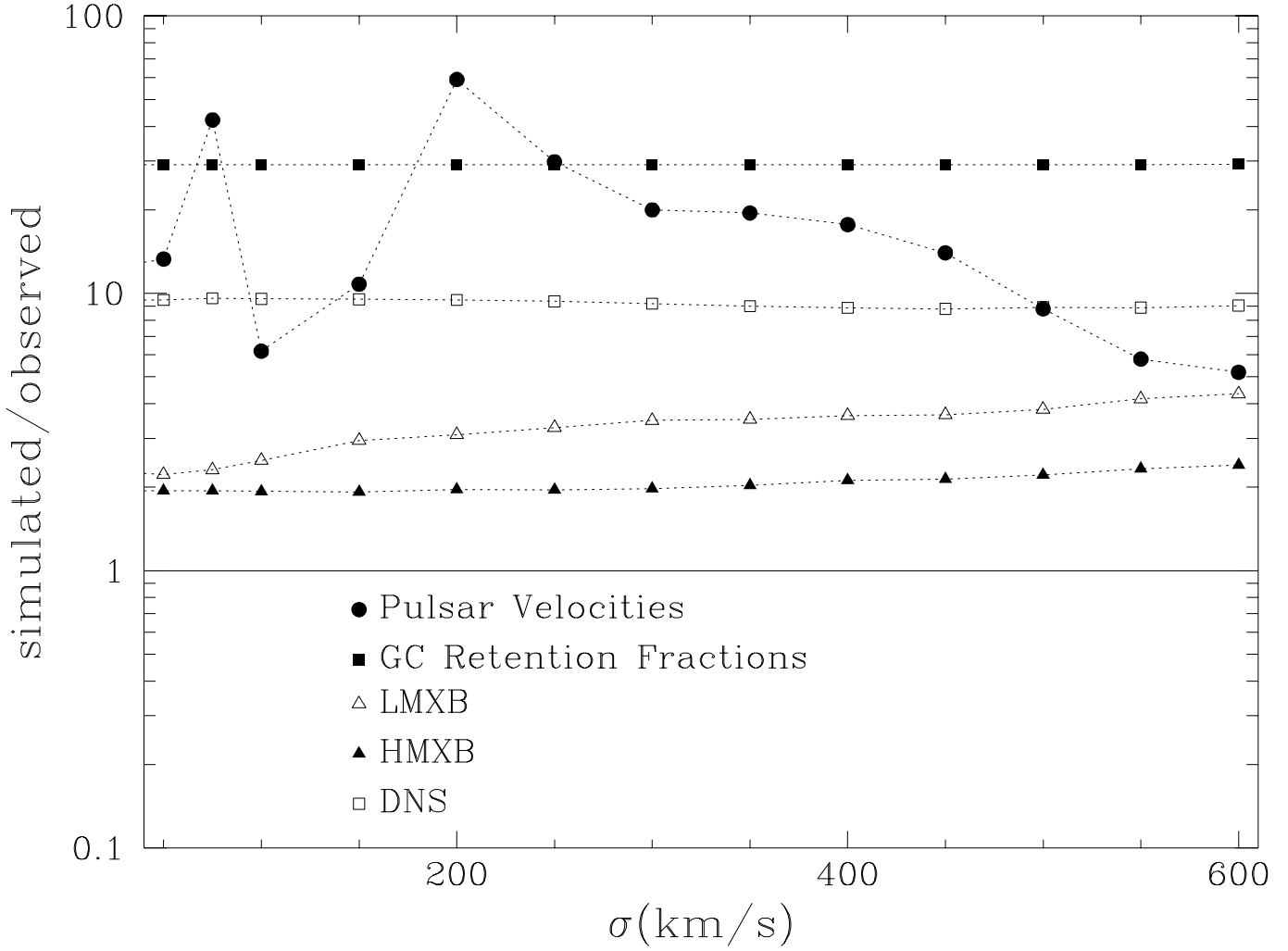


Fig. 16.— Same as Fig 8. with a double-peaked distribution: 30% at 0 km/s and 70% with a flat distribution with a mean at 625 km/s and a dispersion:  $\sigma$ . Again, we use  $q_0 = 0.15$ .



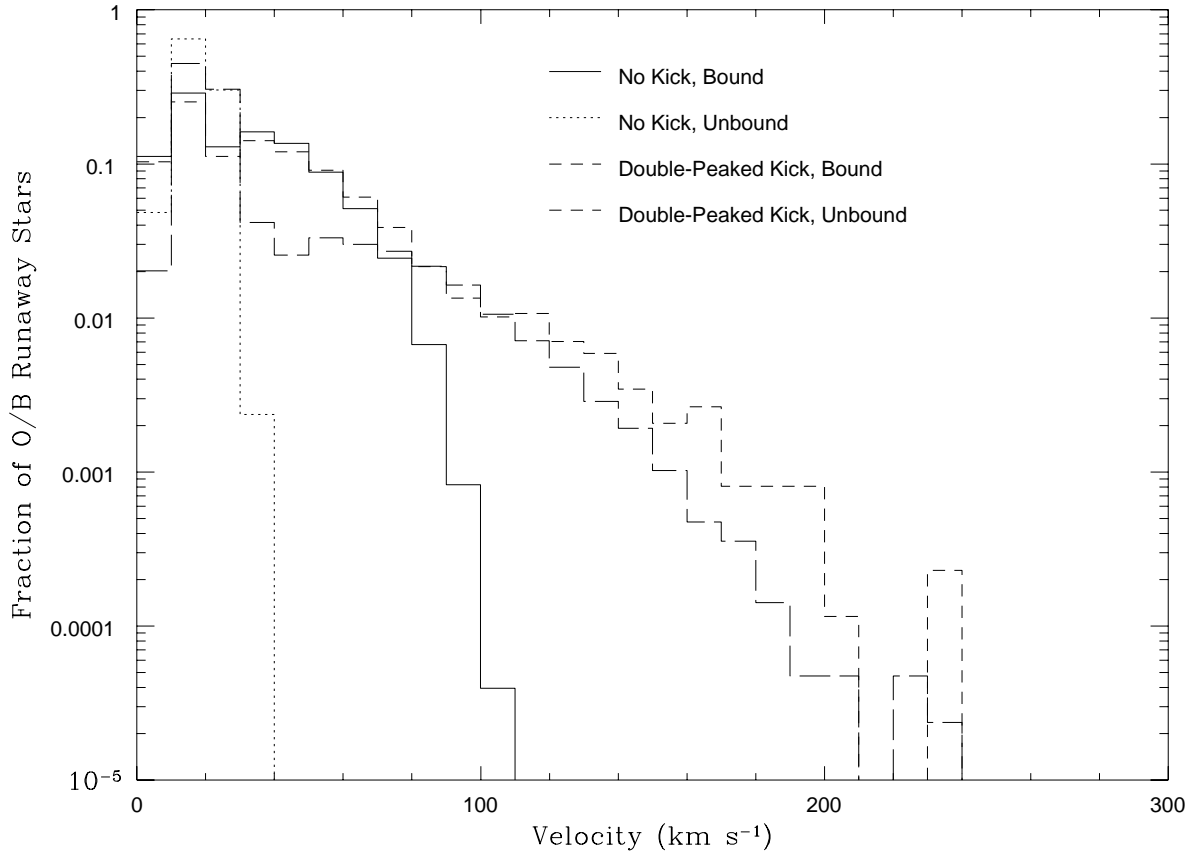


Fig. 17.— The velocity distribution of O/B stars for simulations with no kick (solid line - bound systems, dotted line - unbound O/B stars) and for our best fitting double peaked distribution (long-dashed line - bound systems, short-dashed line - unbound systems.)